INFLUENCE OF AGGREGATES PROPERTIES ON MICROSTRUCTURAL PROPERTIES AND MECHANICAL PERFORMANCE OF ASPHALT MIXTURES

Selinah Busang[a,*], James Maina[a]

[a]Department of Civil Engineering, University of Pretoria, Private Bag X20, Hatfield 0028, South Africa: selbusang@gmail.com

[a]Department of Civil Engineering, University of Pretoria, Private Bag X20, Hatfield 0028, South Africa: james.maina@up.ac.za

*Corresponding author.

Highlights

- Three aggregates were selected to characterise the chemical and physical properties.
- Influence of chemical composition on the strength and shape of aggregate.
- Influence of the strength and shape of aggregate on the microstructural properties was evaluated.
- Influence of microstructural properties to the performance of asphalt mixture was evaluated.
- Normal contact fabric tensor has an excellent linear relationship with mechanical properties.

Abstract

Asphalt mixtures can perform suitably in road and airfield pavements. However, with rapid increases in traffic volumes, harsh climate environments, and heavier loads, there is an increased interest in improving the mechanical properties of asphalt materials through a suitable design of the microstructure of the asphalt mixture. Aggregates' physical and chemical properties significantly influence the interface interaction between aggregates and binders and achieve strong, durable and cost-effective asphalt mixtures. This study prepared the asphalt mixtures from three different aggregate sources, i.e. Granite 1 (GD 1), Granite 2 (GD 2) and limestone (GD 3) and captured the microstructural properties using a charge-coupled device (CCD) digital camera and analysed them by iPAS software. The effect of the daily temperature variation of the environment to the corresponding temperature gradient through the depth of

all asphalt mixtures layers was assessed. The results indicate that sodium oxide (Na_2O) + potassium oxide (K_2O) +calcium oxide (CaO) + silicon (SiO_2) has a significant influence on the electrical conductivity of granite samples at high temperatures and pressure. Marshall, wheel tracking, three-point bending beam, double tension-compression fatigue tests at two periods were conducted to investigate any relationship between the structural performance of the asphalt mixtures and their microstructural properties. Additionally, the normal contact fabric tensor (F) was developed to t evaluate the interlocking of aggregates in asphalt mixtures, and the correlation with the mechanical performance was performed. The results show that the higher amount of silicon and aluminium in aggregates, the better the aggregate texture and the high contact points weight. In addition, high contact points weight has a notable impact on the Marshall stability, rutting depth, dynamic stability, stiffness modulus and complex Poisson's ratio at high and low temperatures. All samples showed good mechanical performance at all temperatures because of their high aggregate particles F.

Keywords: Aggregate properties, Microstructural properties, Mechanical performance of asphalt mixture

1 Introduction

Recent developments in promoting easy trading between Southern African Development Countries (SADC) have renewed interest in constructing highways to international standards. The construction activities are stimulating the SADC's economic and social development. Most of these highways are constructed using asphalt mixtures because of their low cost, accessibility and ease of maintenance and repair compared to cement concrete [1]. However, different sections of these highways have different service lives due to their long distances; they have been constructed using different aggregates obtained from different quarries and rock sources and are exposed to different environmental conditions. In this regard, it is vital to

understand the contribution of aggregates properties to the microstructural properties, hence the mechanical performance of asphalt mixtures.

Decent quality pavement structures are critical to ensuring the long service life of road networks and airfields. Such pavements should meet the requirements for mechanical (structural) performance such as fatigue cracking and rutting as well as functional performance such as smooth ride quality. These pavement structures must withstand high traffic volumes and adequately transmit repeated traffic load to the underlying layers. The microstructure of the asphalt mixture has been used successfully to simulate or predict the mechanical performance to obtain decent quality pavement [2]. Several studies highlighted that besides the method of compaction and compaction energy, aggregate chemical and physical properties (such as aggregate size, orientation, morphology, texture, shape) have a significant influence on microstructural properties, hence the mechanical response and performance of asphalt mixture [1], [3], [4]. Han et al. [5] conducted a study on the effect of microstructure with different aggregate morphology on the dynamic modulus of asphalt mixture. They found that aggregate morphology has a major influence on the dynamic moduli of asphalt mixture. Yang [6] studied the effects of the shape and angularity of coarse aggregates on the microstructure as well as the mechanical performance of asphalt mixtures. They found that asphalt mixtures containing aggregates with higher shape indexes and lower angularity have higher creep deformation and low dynamic modulus. Kuang [7] mentioned that the average angular coefficient on microstructure demonstrates a positive linear correlation between the dynamic stability and freeze-thaw split strength ratio of the asphalt mixture. Angularity coefficient is the aggregate particle shape evaluation method. It is mainly the quantitative characterisation of the angularity and roughness of aggregate particles. The mean angularity coefficient of several aggregates particles is obtained from the void ratios of aggregate particles tamped based on different times. Gao [8] highlighted that a microstructure with more aggregate particles with

high angularity is harder to compact the asphalt mixture but that it provides better skid resistance. Ge et al. [9] used microstructures of coarse aggregates with various particle sizes and shapes under various abrasion cycles. They discovered that the small size ranges of aggregates have a very good surface texture, but they easily get damaged during the abrasion cycles process. Wang et al. [10] examined the influence of morphological properties of coarse aggregate on the microstructures. They found that the aggregate particles' fractal dimension which was measured by the slit island method, has a better linear correlation with the dynamic stability of asphalt mixtures at high temperatures. The coarse aggregates with higher angularity have shown stronger stability at high temperatures.

Asphalt mixture is constituted of bitumen binder, mineral filler, aggregate and voids. Its mechanical performance is influenced by the interactions of its various constituent materials, such as the interaction between bituminous binder and filler and the interaction between bitumen mastic and aggregate. However, not much has been done to investigate the effect of aggregates' chemical and physical properties on the mechanical performance of asphalt mixtures. Therefore, the study aims to investigate the influence of the chemical and physical properties of the aggregates on the microstructural properties of asphalt mixture. Three different aggregate types from various quarries with different morphologies, compositional oxides and strengths were used to prepare asphalt mixtures.

- All three aggregate types' mineral composition was measured using X-Ray Spectrometry (X-Ray Spectrometer Model Rigaku RIX 3000).
- The iPAS software (Image Processing Analysis System) centred on DIP was utilised to obtain the asphalt mixture's microstructural properties. To capture the cross-sectional images of the microstructures, a two-dimensional (2D) image processing approach based on a charge-coupled device (CCD), using digital cameras was utilised [3], [11].

The following information was obtained: contact properties, orientation, and aggregate distribution.

- Constructed Fabric tensors were used to evaluate the interlocking of aggregates in asphalt mixture.
- The study used testing parameters including Marshall stability, dynamic stability and bending stiffness modulus and complex Poisson's ratio to assess the influence of the chemical and physical properties of aggregates on the mechanical performance of the asphalt mixtures.

The main objectives of the work presented in this paper were as follows, and the scope is given on the flow chart by Fig 1:

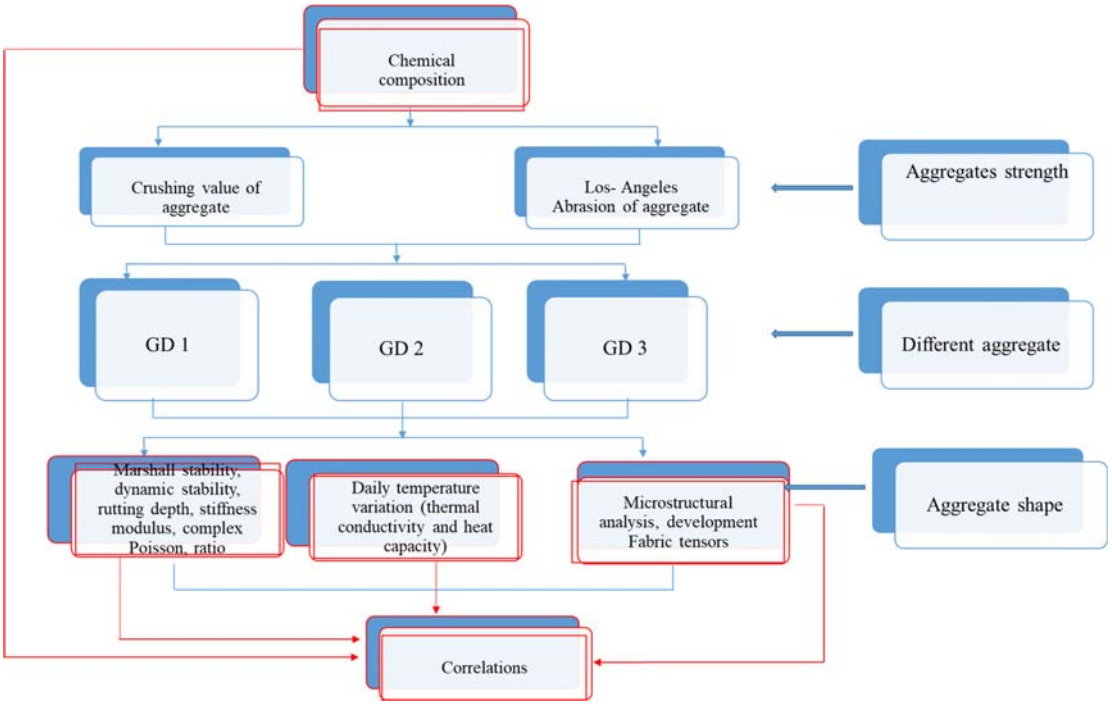

Fig 1: The flow chart of this research.

1.1 Rock mineral in Botswana

Most aggregates in Botswana are granite or limestone, and these are used as the traditional materials to produce asphalt mixtures. The composition of the minerals that make up

aggregates based on their hydrophilic or hydrophobic properties and their relationship with bitumen is also important in moisture damage. High-carbonate aggregates (hydrophobic or basic), like limestone, are easier to coat. These aggregates create a great bonding with the bitumen compared to aggregate with a high percentage of silica, i.e. granite (acidic or hydrophilic aggregates), which is the main reason for the acidity of the bitumen [12].

Granite aggregates are acidic igneous rock, in mineral composition was characterised by: quartz (>50 %); plagioclase; feldspars; mica. Chemical composition of granite: SiO_2; K_2O; $Al2O_3$; Fe_2O_3, TiO_2; FeO [13]. Granite is classically an acidic aggregate, with large texture depth surface microstructure, more texture, and high resistance to wear. Granite also has many physical properties, such as resistance to polishing, which is superior to limestone [14]. The interaction of granite and bitumen is a significant factor in developing the microstructure of asphalt mixtures. The granite aggregate whose mineral particles are relatively small has a higher adhesion. When the mineral particles of the granite are relatively large, with certain minerals glossy crystal faces, it has poor adhesiveness with bitumen [15]. Dense marble-like limestone comprises either calcite or dolomite, while dolomite is the most common among the two. The chemical formula of limestone includes the following compounds: $CaCO_3$; $MgCO_3$ [13]. The interaction of these compounds has a favourable impact on the adhesion of bitumen to the mineral surface [16].

1.2 Anisotropy of asphalt mixtures

The arrangement and organisation of particles and other constituents of microstructures within a soil mass have been named fabric. Like other granular materials, the asphalt mixture is allied with different microstructural quantities such as the elongated particle orientation direction, contact normal vectors, branch vectors, and void vectors. It has been widely observed in experimental tests [17], [18] and numerical simulations [19], [20] that the fabric of asphalt

materials is anisotropic and are in two types. (I) inherent anisotropy of an asphalt mixture as results from aggregates shape. During the compaction of asphalt mixtures, the aggregates have a tendency to “lie flat” the main axis, which is the longest diameter of the aggregate, has a preferential direction in the horizontal plane [21], [22]. (II) The stress-induced anisotropy is due to a crack growth induced by loading [23]. When the crack surface area gradually grows, the material will slowly lose the intact, resulting in modulus degradation. The rate at which the crack growth varies in various directions, resulting in various modulus degradation in various directions and producing stress-induced anisotropy in the asphalt mixture [23], [24]. Fabric anisotropy and its evolution have an important influence on the mechanical properties of microstructure [17], for example, elastic moduli [25], shear strength [26], and dilatancy [27]. These mechanical performances of asphalt mixture are closely related to the stability and buckling of force chains at a mesoscopic scale and sliding and rolling at contacts, accordingly controlled by the aggregate gradation and compaction. Related literature developed several fabric tensors to determine the fabric features by recitation the spatial distribution of various microstructural quantities and a statistical demonstration of the microstructural fabric, and it was later reworked by Li et al.[28]

2 Material and data

2.1 Aggregates

The selection of aggregates was based on three principles: (i) most rock-forming minerals must be of silicate or carbonate origin; (iii), the deposits of the selected rocks must be in large quantities. In Botswana, the quarries that complied were located more than 500 km apart. Table 1 shows the gradations of local aggregate: (I) Granite (GD 1) supplied by a Belabela quarry in Mokolodi, the southern part of Botswana; (II) Granite (GD 2) supplied by a quarry in Sekoma, a desert area in Botswana and Limestone (GD 3) supplied by a quarry in Chobe district, the northern part of Botswana. The mineral composition and oxide constituents of GD 1, GD 2 and

GD 3 were obtained from the mineral fillers (75µm) using X-Ray Spectrometer Model Rigaku RIX 3000 as given in Table 2, and the strength properties, bulk specific gravity, and apparent relative gravity are in Table 3.

Table 1: Gradation of 3 types of aggregates.

Sieve/ mm	**16**	**13.2**	**9.5**	**4.75**	**2.36**	**1.18**	**0.6**	**0.3**	**0.15**	**0.075**
Gradations					Passing rate /%					
GD 1	100	59	34	27	23	19.7	14.5	11.3	9.7	6.2
GD 2	100	70.3	48.3	28.1	22	19.3	14.2	11.5	9.8	6.2
GD 3	100	74.6	57.2	41.6	24	18.2	13.4	10.7	9.4	6.2

Table 2: Chemical composition of aggregates

Oxides	**GD 1**	**GD 2**	**GD 3**
SiO_2	70	67	1.38
Al_2O 3	16	15.3	0.72
K_2O	6.1	7.4	
Fe_2O_3	2.3	2.9	0.12
CaO	2.2	2.6	56.1
Na_2O	1.9	2.3	
MgO	0.88	0.91	0.13
TiO_2	0.3	0.32	
P_2O_5	0.18	0.24	
MnO	0.18	0.23	
SO_3	0.12	0.16	0.21
Rb_2O	0.058	0.09	
BaO	0.049	0.05	

Table 3: Aggregate particles properties

GD 1											
	Coarse aggregates				Fine aggregates.						Standards
Sieve size/mm	16	13.2	9.5	4.75	2.36	1.18	0.6	0.3	0.15	0.075	
Bulk specific gravity /(g/cm3)	2.689	0.693	0.691	0.7							T0304
Apparent relative gravity /(g/cm3)					2.76	2.67	2.684	2.755	2.742	2.733	T0304
Crushing Value (CV)					19.2						T0316
Los-Angeles Abrasion (LAA)					16.11						T0317
Water Absorption (WA)					1.49						T0304
Flakiness Index (FI)					10						0T312
Roundness Index (RI)					0.73						
GD 2											
	Coarse aggregates				Fine aggregates.						
Sieve size/mm	16	13.2	9.5	4.75	2.36	1.18	0.6	0.3	0.15	0.075	
Bulk specific gravity /(g/cm3)	2.65	0.682	0.688	0.701							T0304
Apparent relative gravity /(g/cm3)					2.66	2.65	2.654	2.705	2.731	2.712	T0304
Crushing Value (CV)					18.78						T0316
Los-Angeles Abrasion (LAA)					17.02						T0317
Water Absorption (WA)					1.62						T0304
Flakiness Index (FI)					14.2						0T312
Roundness Index (RI)					0.61						
GD 3											
	Coarse aggregates				Fine aggregates.						
Sieve size/mm	16	13.2	9.5	4.75	2.36	1.18	0.6	0.3	0.15	0.075	
Bulk specific gravity /(g/cm3)	2.61	0.674	0.676	0.681							T0304
Apparent relative gravity /(g/cm3)					2.62	2.63	2.65	2.685	2.703	2.686	T0304
Crushing Value (CV)					18.66						T0316
Los-Angeles Abrasion (LAA)					16.72						T0317
Water Absorption (WA)					1.51						T0304
Flakiness Index (FI)					14.15						T0312
Roundness Index (RI)					0.58						

2.2 Asphalt

The study used bitumen bought from Tosas Botswana, and the properties are given in Table 4. The properties of asphalt were assessed per the relevant requirements of the Test Procedure for Highway Engineering Asphalt and Asphalt Mixtures (JTJ 052-2000) [29].

Table 4: Bitumen properties

Property	Specification	Test value
Penetration (25 °C), 0.01 mm	60/80	70.1
Softening point (ring and ball method)/°C	70 Min.	89.1
Ductility (5 °C), cm	≥100	>100
Brookfield Viscosity (135 °C), Pa.s	3.0 Max.	2.373
Flash Point (COC), °	260 Min.	298
RTFOT (163 °C, 85min), Quality /%, no	≥±0.8	
Residual penetration ratio (25 °C) /%	≥61	69.3
Residual ductility (10 °C)/ cm	≥04	7
Residual ductility (15 °C)/ cm	≥15	32.1
Density (15 °C)g/cm3	Measured	1.057

2.3 Daily environmental

A parametric study was performed to evaluate gradation effects on the asphalt mixture's thermal conductivity and heat capacity. Daily environmental information was collected from Botswana Environment Statistics Climate Digest in this study, forming two sets of data involving cold environment representing winter and hot environment representing summer [30]. Other data used involved the material properties such as the absorptivity ($\alpha = 1 - \beta$); the emissivity (e) of the top layer; the thermal conductivity (k); and the volumetric heat capacity (c) of asphalt mixture. For all materials, the absorptivity ($\alpha = 0.9$); the emissivity (0.85) [31].

3 Sample preparation and experimental procedure

The anisotropy of a material is the property of being directionally dependent. The anisotropy of an asphalt mixture can be described as the variation in physical properties, such as modulus and Poisson's ratio, when the asphalt mixture is measured in different directions.

Table 5: Number of replicates per test

Mixtures	Tests	Number of Replicates
GD 1 GD 2 GD 3	Marshall stability	3
	Wheel tracking stability	3
	Bending test	10
	Complex Poisson ratio	3

3.1 Marshall stability

To define the deterioration of toughness and the breaking point load of the asphalt mixture, samples were compacted at a temperature range of 180 ± 0.5°C. First, the samples were isothermally conditioned for 30 min; the samples were put in a constant temperature water bath until to the temperature of 60 ± 1°C. Then samples were set for the Marshall tester machine and a constant deterioration rate of 50.8 mm/min. The maximum load achieved (i.e. the stability) and the deflection at which the maximum load occurs (i.e. the flow) were recorded on the Marshall Testing Machine [32]. Marshall specimens were prepared and tested according to the standard test method specified in ‘‘Test Methods of Asphalt and Asphalt Mixture for Highway Engineering (JTG E20-2011)”[29].

3.2 Wheel tracking test

Asphalt mixture slabs of 300 mm × 300 mm × 50 mm dimensions were prepared and compacted by a laboratory automatic rolling compaction machine and left for curing. For insulating purposes, all samples were kept for five hours at a temperature of 60 ± 1°C on a wheel tracking machine test bench. In this study, a temperature of 60°C was selected [33]–[35]. Fig 2 shows the wheel was traversed on the centre of the sample in both directions for an hour. The wheel was of a diameter of 200 mm and 50 mm wide, also composed of rubber of a small thick 15 mm. The wheel and sample contact pressure was 0.7 MPa, and the entire forced load was 780 N at a speed of was 42 ± 1 cycles/min in one direction (21 cycles in two

directions). Dynamic stability (DS) was determined using Eq. (1) [3], [36]. The wheel tracking test was performed according to JTG E20-2011 [29].

$$DS = \frac{(t_2 - t_1) \times N}{d_2 - d_1} \times C_1 \times C_2 \quad (1)$$

where; d_1 and d_2 the extent of deformation at the time t_1 (mm, 45 min) and t_2 (mm, 60 min) respectively; N denotes the rapidity of tire 42 passes per 60 seconds; C1 denotes the coefficient of the alteration connected to the machine, and C2 is the coefficient of alteration connected to the samples (for this study, it was 1.0).

Fig. 2: Wheel tracking test

3.3 Bending test

A three-point bending test evaluated the bending failure of the asphalt mixture. Rectangular beam samples of dimensions: length (L = 250 mm), width (b = 30 mm) and height (h = 35 mm) for each type of aggregates were prepared. The samples were soaked in a thermostatic water bath for 1 hour. Then they were loaded at a rate of 50 mm/ min at 10 ± 0.5 °C, and 0 ± 0.5 °C. the procedure T0715-2011 of the Standard Test Methods of Asphalt and Mixtures for Highway Engineering (JTG E20-2011) [29]. Eq. (2) [3] was used to calculate flexural tensile strength

R_B, Eq. (3) [3] was used to calculate the maximum flexural tensile strain ε_B, and Eq. 4 [37], for the bending stiffness modulus S_B.

$$R_B = \frac{3 \times L \times P_B}{2 \times b \times h^2} \tag{2}$$

$$\varepsilon_B = \frac{6 \times h \times d}{\varepsilon_B} \tag{3}$$

$$S_B = \frac{R_B}{\varepsilon_B} \tag{4}$$

where, L represents the length b, represents the width and h represents the height of the samples, P_B represents the maximum load at the time of sample failure, d represents the mid-span deflection at the time of breakage and S_B represents the bending stiffness modulus

3.4 Complex modulus and complex Poisson's ratio

Other anisotropy properties of the asphalt mixture involve; the complex modulus and complex Poisson's ratio. The properties are used to describe the viscoelastic linear response and are obtained by subjecting the samples to the sinusoidal loading. Using the tension-compression tests such as the axial stress σ_1, axial strain ε_1 and radial strain ε_2 as a function of time (t) by Eqs. (5) to (7) [38], the complex modulus E^* and the complex Poisson's ratio v^* are obtainable using Eqs. (8) and (9) [38].

$$\sigma_1(t) = \sigma_{01}\, sin\, sin\, (2\pi f t + \phi\sigma_1) \tag{5}$$

$$\varepsilon_1(t) = \varepsilon_{01}\, sin\, sin\, (2\pi f t + \phi\varepsilon_1) \tag{6}$$

$$\varepsilon_2(t) = \varepsilon_{02}\, sin\, sin\, (2\pi f t + \phi\varepsilon_2) \tag{7}$$

$$E^* = \frac{\sigma_{01}}{\varepsilon_{01}} e^{j(\phi_{\sigma 1} - \phi_{\varepsilon 1})} = |E^*|\, e^{j\phi_E} \tag{8}$$

$$v^* = \frac{\varepsilon_{02}}{\varepsilon_{01}} e^{j(\phi_{\varepsilon 2} - \phi_{\varepsilon 1})} = \frac{\varepsilon_{02}}{\varepsilon_{01}} e^{j(\phi_{\varepsilon 2} - \phi_{\varepsilon 1} - \pi)} = |v^*|\, e^{j\phi_v} \tag{9}$$

where, f is frequency; amplitudes σ_{01}, ε_{01} and ε_{02} refer to the stress, axial strain and radial strain, respectively; $\phi_{\sigma 1}$ refers to phase angle stress, $\phi_{\varepsilon 1}$ and $\phi_{\varepsilon 2}$ refer to axial and radial strain, respectively; $j^2 = -1$ is complex number, $|E^*|$, ϕ_E and $|v^*|$, ϕ_v refer to the norm and phase angle of the complex modulus and complex Poisson's ratio, respectively. While the phase lag between σ_1 and ε_1 is characterised by ϕ_E and ϕ_v refers to the phase lag between ε_1 and opposite of ε_2.

Fig. 3 is a schematic of the test equipment used, where all parameters required to determine the complex modulus and complex Poisson's ratio are measured [38]–[40]. Briefly, the principles followed were: samples of height and diameter of 140 mm and 75 mm, respectively, are fixed with glue on the load plates. The axial strain was measured using three extensometers, while the radial strain was obtained from two non-contact sensors. It is assumed that the strain is homogeneous in the middle of the samples. Therefore, extensometers (75mm length) were placed every third part and non-contact in the centre part of the sample to accurately capture the strain.

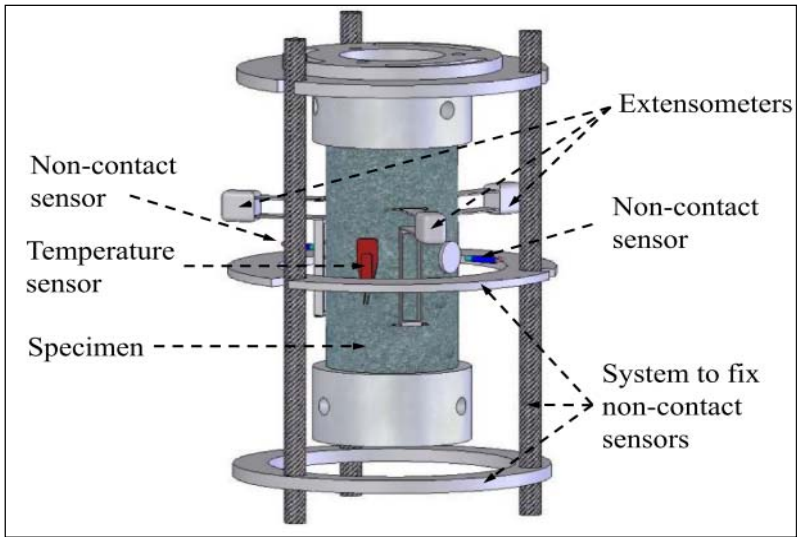

Fig. 3: Cylindrical samples set for axial and radial strain measurements

3.4.1 Applied time - temperature and cyclic loading on samples

The investigation on how time-temperature affect the complex Poisson's ratio was performed. The investigation was performed at a temperature range, 25°C to 50°C. The frequency between 0.01Hz and 10Hz, under strain-controlled with the strain amplitude of about 50 μm/m. On the other hand, the two tension-compression fatigue tests were carried out to assess the influence of cyclic loading on the complex Poisson's Ratio.

3.5 Image analysis and microstructural analysis

The samples were saw-cut using a universal cutting machine G210. Samples were sawed along the horizontal direction, and the slab samples were subdivided into thinner cross-sections. Accordingly, each Marshall sample was saw-cut to 36 circular cross-sections, and each slab sample was saw-cut to 24 rectangular cross-sections, as illustrated in Fig. 4.

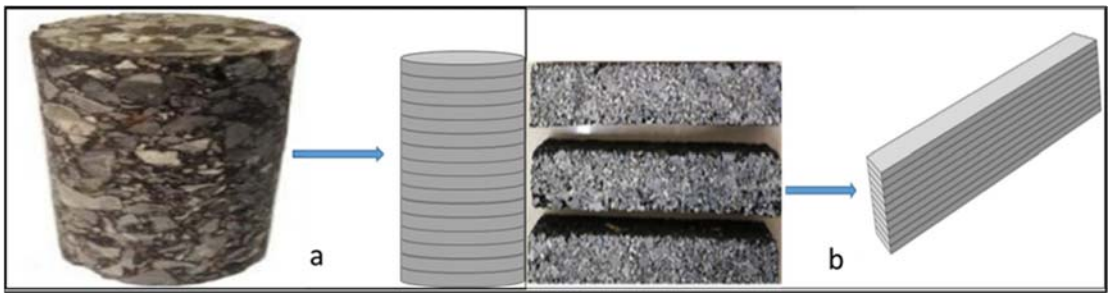

Fig 4:Illustration of sawed samples

The recent digital industry is using two processing methods to analyse asphalt mixture images: the three-dimensional (3D) and the 2D image analyses methods are based on X-ray and charge-coupled device (CCD), respectively [3], [41]. This study selected the CCD digital camera-based photography method to acquire various colours and differentiate numerous materials with high-precision cross-sectional photographs at a lower price, quick imaging, and user-friendly equipment [3], [41].

Several studies worked on the theory of "join pair" in the examination of the 3-D interaction amongst aggregate particles and considered that two adjacent aggregates contact each other

when the boundary pixel distance is less than a certain threshold [3], [42]. Nevertheless, the asphalt mixture has three-phase constitutes; taking images using a digital camera may result in some errors, for instance, influence the acuity of the sample edge of the image caused by the spatial domain's noise. In this study, as shown in Fig. 5, the following steps were involved in minimising the errors:

I. The cross-section images of sawed parts of samples were captured using a CCD digital camera, followed by iPAS [8]. Initial analyses were achieved by filtering denoising, image improvement, and obtaining the threshold at (2.36 mm) intervals.

II. The multi-goal versatile window division calculation was used to capture the aggregate perimeter primarily then the image was set for binarisation.

III. Afterwards, virtual screening was performed on the binarised image slices to capture all ranges of aggregates and label them using numbers.

IV. Lastly, the spatial closeness relationship between adjacent aggregates was measured. Total contact points numbers (N) were counted, the contact orientations were marked, contact line and total contact line length were calculated.

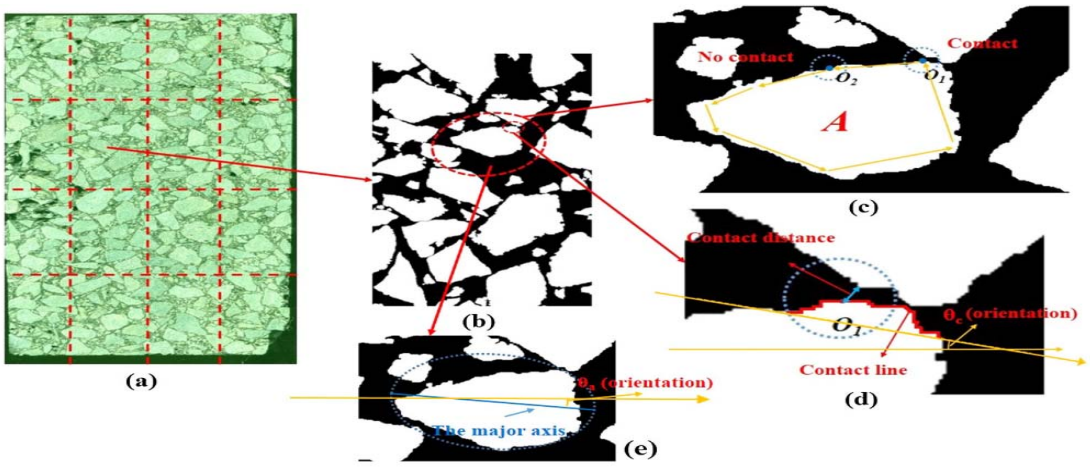

Fig.5: Image analysis and processing focus on coarse aggregate particles (a) an example section of UTA-10 with green filter, (b) zoomed binary image, (c) contact judgment processing, (d) definition of the contact indices, (e) orientation [43]

3.5.1 Contact mapping analyses by fabric tensors

Several studies used the internal structure index (ISI) to evaluate the interlocking of aggregates in asphalt mixture by combining the contact line length and contact orientation [3], [44]. This study maps the interlocking of aggregates in asphalt mixture by using Fabric tensors, which quantifies the directional distribution of microstructural properties concisely, which is critical to use in constitutive modelling. Another way to define microstructural fabric based on the aggregate gradation packing is to use the plane that describes the direction of the contact, as illustrated in Fig. 6. This plane can be described as vertical to the contact point and the plane that is tangent to the particles in contact. Contact normal vectors are defined by the two-unit vectors n^c and -n^c. The number of aggregates in a microstructure was denoted by N_a aggregates and contact points by N_c. Some methods considered mapping a fabric tensor to a directional in a comparative frequency distribution of contact normal normally using probability density function $E(n)$ [45]. The second-order spherical harmonic sequence for the 3D asphalt mixture can be reduced to Eq (10) [19].

$$E(n) = \frac{1}{4\pi}(1 + F{:}\, n^c \otimes n^c) \tag{10}$$

where $\otimes$ represents a dyadic product, and as given in Eq. (11), F represents traceless tensor regarded as the second-order fabric tensor of the third type based on unit contact normal [46]. Basically, the fabric tensor (F) can be determined from the second-order tensor N. In this study, F is used to evaluate the anisotropy properties because of the ability to obtain the most important microstructural properties that influence the asphalt mixture performance based on a small number of parameters [47]. Based on this definition of contact normal plane and on contact normal vectors, the fabric tensor for contact normal vectors (contact normal fabric) can be defined as:

$$F = \frac{15}{2}(N - \frac{1}{3}I) \tag{11}$$

where I represent each second-order tensor; N represents a function of the discrete contact normal tensor n in aggregate gradation parking, see Eq. (12) [48].

$$N = \frac{1}{N_c} \sum_{c \in N_c} n^c \otimes n^c \tag{12}$$

In this study, weight examination was used to determine the relationship between the aggregate and mechanical properties, as already mentioned.

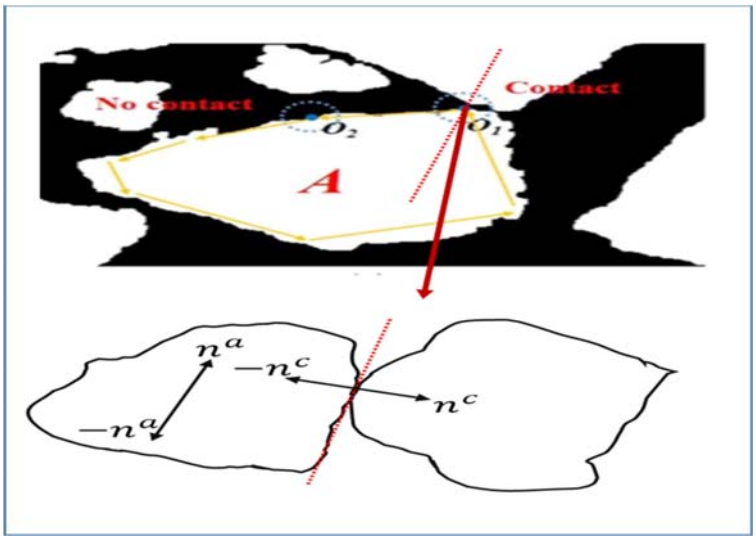

Figure 6:Vectors that describe the microstructure of asphalt mixture

3.6 Grey relational analysis method

Grey relational analysis provides the opportunity to optimise more than one of an asphalt mixe's mechanical performance properties. The method brings aspects such as: (i) experimental design and its application, (ii) Signal- noise (S/N) Ratio calculation, (iii) decision matrix creating, (iv) data normalisation, (v) weighting of normalised, and (vi) Ranking points. The calculation procedures were determined with MATLAB.

Table 6: Symbol list for Grey relational analysis method [49]

Steps	Definitions		Equations
Step 1.	The reference sequence of length n is as follows		$x_0 = (x_0(1), x_0(2), x_0(3), \dots x_0(n)$ (1)
Step 2.	Data Normalization	The Larger -The Better	$x_i(k) = \frac{x_i^0(k) - min\, x_i^0(k)}{\max x_i^0(k) - min\, x_i^0(k)}$ (2)
		The small - The better	$x_i(k) = \frac{max\, x_i^0(k) - x_i^0(k)}{max\, x_i^0(k) - min\, x_i^0(k)}$ …… (3)
		The Nominal - The Better	$x_i^0(k) = 1 - \frac{\lvert x_i^0(k) - x^0 \rvert}{max\, x_i^0(k) - 1}$ (4)
Step 3.	The m number series going to be compared with *xo* series		$x_i = (x_i(1), x_i(2), x_i(3), \dots, x_i(n),$ $i = 1,2,3 \dots m$ (5)
Step 4.	Grey Relational Coefficient is calculated.		$\varepsilon(x_0(k), x_i(k)) = \frac{\Delta_{min} + \xi \Delta_{max}}{\Delta_{0i}(k) + \xi \Delta_{max}}$ (6) $\Delta_{0i}(k) = \lvert x_0(k) - x_j(k) \rvert$ (7) $\Delta_{min} = min_j min_k \lvert x_0(k) - x_j(k) \rvert$ (8) $\Delta_{max} = max_j max_k \lvert x_0(k) - x_j(k) \rvert$ (9)
Step 5.	Weights Determination		W
Step 6.	Grey Relational Degree is calculated by Equation	If impact on the performance of the output is equal,	$\gamma(x_0, x_i) = \frac{1}{n} \sum_{k=1}^{n} \varepsilon(x_0(k), x_i(k))$ (10)
		If impact on the performance of the output is not equal,	$\gamma(x_0, x_i) = \frac{1}{n} \sum_{k=1}^{n} w_k(x_0(k), x_i(k))$ (11)

Where $x_i(k)$, = after normalisation i series k. value, $x_i^o(k)$ =i series k, min $x_i^o(k)$= minimum value in i series, max $x_i^o(k)$= maximum value in i series, x^o= desire deal value, x_i = m series with x^o series, $\varepsilon(x_0(k), x_i(k))$= grey relational coefficient at poit k.k.k. ranking in n length series, k = 1,2,…,n, j = 1,2,.., m, ξ = a coefficient between (0,1), Δ_{min}=minimum value in the series, Δ_{max}= maximum value in the series, $\Delta_{0i}(k)$ = k value in the series, $\gamma(x_0, x_i)$ = grey relation degree in i. rank, W_k= total weight must be 1.

4 Results and discussions

In this study, the physical and chemical properties of aggregate particles were captured to evaluate their influence on microstructural properties. The microstructural properties were used to predict the mechanical performance of asphalt mixtures. As indicated in Table 2, the general chemical oxide composition of the GD 1 and GD 2 as granite samples have shown that silicon, calcium, and aluminium are the three major elements in the granite aggregate particles. The silicon and aluminium concentrates were approximately 16% to 70% by weight, respectively. The high amount of silicon, aluminium and calcium suggests high pozzolanic content and hence fewer mineral voids. Yagüe et al. [50] used chemical and morphological analysis of granite sawdust waste as pozzolan material. The results suggested that the granite sawdust rich in silicates (quartz, feldspars, phyllosilicates) provides commercial ordinary Portland cement (rich in alkalis). Also, it was observed that when Si and Al are the major constituents, the properties of cement are improved to generate a pozzolanic cement of an ecological nature. Also, the study found that alkaline elements contents are larger than 5%, the acid composition and the particle size has shown noteworthy pozzolanic activity. The major chemical oxide composition of GD 3 is calcium and silicon, which also suggest a high strength. Table 3 provides the aggregates' shape and properties; GD 1 has shown the highest values of CV and LAA, followed by GD 2 and the least values for GD 3. The values indicate high strength as a high amount of silicon and aluminium provides good hardening with small crystallinity of the rock. Also, GD 1 has shown the lowest value of WA and the highest value of FI. This means GD 1 does not easily absorb water because the crystals are well compacted due to the high amount of silicon and aluminium. It can also be seen that GD 2 has a high amount of FI than GD 3; the higher the FI and lower WA, the stronger is the material. Calcium oxide (CaO) and silicon dioxide (SiO2) minerals result in a fundamental change in the hydrophilic or hydrophobic properties of the asphalt mixture. The higher the silicon dioxide content, the

greater the hydrophilicity of aggregates, and vice versa. Conversely, the higher the percentage of the calcium oxide mineral, the better the hydrophobicity of the aggregates, and vice versa [51].

The three important parameters, the sum of contact points N_c, the contact orientation to the next corresponding contact aggregate and the contact line were captured based on the optimal contact distance threshold (0.5428 mm), using iPAS software [3], [52]. The distribution of contact line orientation at intervals from angle 15°C to 90°C for all samples are presented in Fig 7. It can be seen that the concentrates of the orientation of contact lines of various mixtures increased with increasing the angle range. For all mixtures, the percentage concentrates of the orientation of contact at angles between 75° and 90° were high, and the orientation percentage reduces as the angles reduce. In contrast, Fig. 7 shows that the percentage distribution contact length of all samples. The contact line length was divided into five different ranges, 0. 5 – 1, 1 – 3. 5, 3.5 – 8, 8 – 12 and >12, and these were used to determine the total contacts line length. The graph indicates that the range of 1–3 m has the highest contact length line for all mixtures. Fig. 8 demonstrated that GD 1 has the highest percentage contact line length followed by GD 2 while GD 3 showed the lowest percentage.

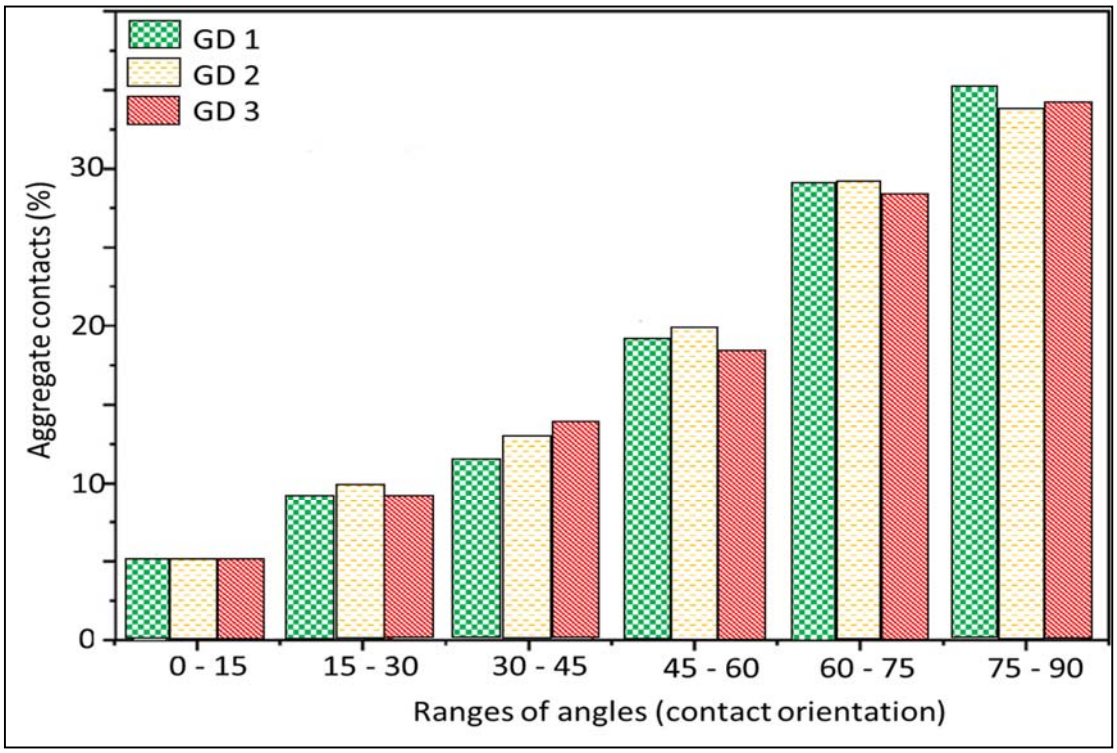

Fig 7: Range of contact orientation of different gradations

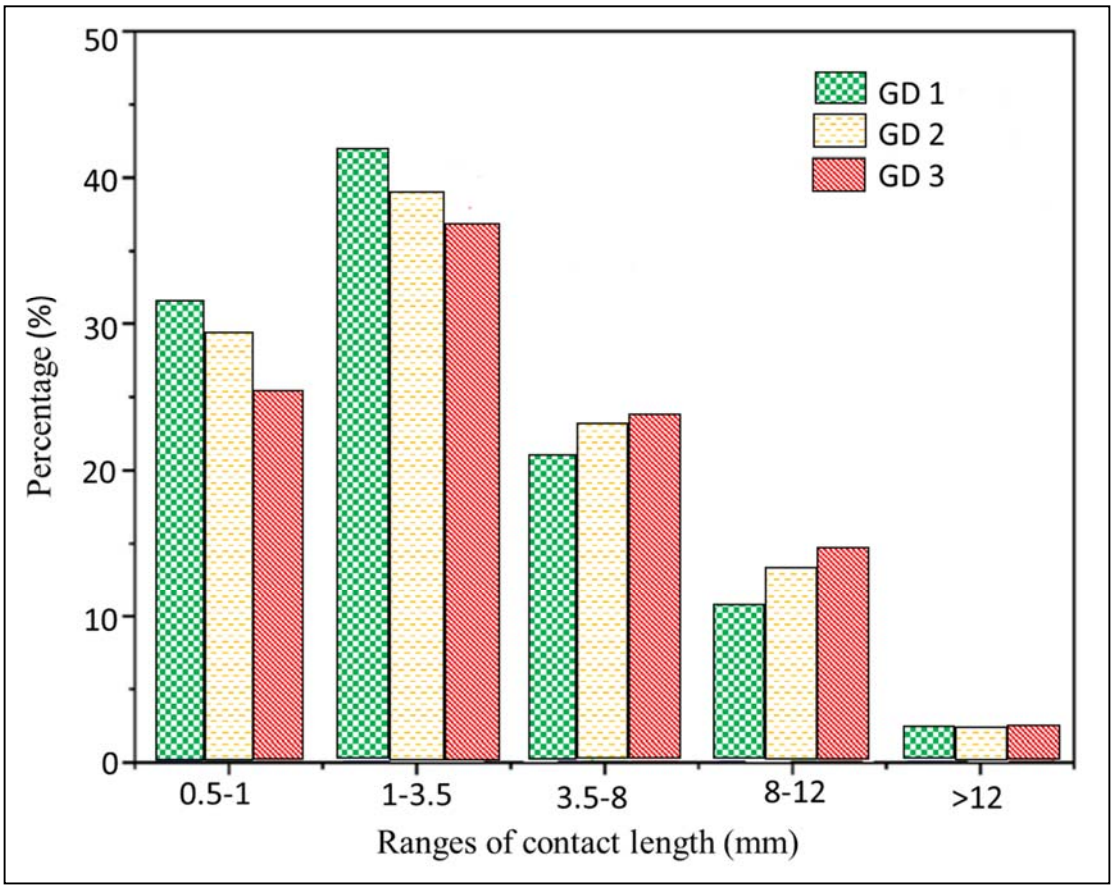

Fig. 8: Range of contact length for different gradations

Several factors that influence the thermal conductivity of aggregates are rock origin and deposition environments and related lithology, mineralogy and texture, and thermal state and as well as thermodynamic conditions [53], [54]. The microstructural properties of asphalt mixture such as aggregate size, contacts number, aggregate contact line length and air void contribute to thermal conductivity and volumetric heat capacity [31]. The effect of contact line length and chemical composition on all mixtures' thermal conductivity and volumetric heat capacity was assessed. Figs. 9a, 9b and 9c present the relationship between the minimum and maximum thermal conductivity trends and minimum and maximum volumetric heat capacity trends for all samples. It can be seen that the minimum thermal conductivity trends are proportional to the minimum volumetric heat capacity trends. A similar observation can be seen that maximum thermal conductivity trends are almost the same as maximum volumetric heat capacity trends. The effects of thermal conductivity and heat capacity on the pavement surface temperature are almost similar to both trends for both samples. Since the volumetric heat capacity is a scalar, it is therefore expected that the anisotropic properties of thermal diffusivity to be similar to those of thermal conductivity. In this regard, the results suggest less than 5% of the anisotropy in the thermal conductivity and thermal diffusivity. Generally, the amplitude of the pavement surface temperature variation decreases with the increase of both thermal conductivity and heat capacity. It can be seen that GD 1 exhibits the highest thermal conductivity, followed by GD 2, while GD 3 has the lowest thermal conductivity, which suggests that the heat was easily conducted between aggregates as a result of a high percentage of contact line length. The higher the thermal conductivity of the asphalt mixture could enhance the heat sink effect of the asphalt mixture and make urban heat islands indifferent from flexible pavement researchers' perspectives. Dai et al. [55] highlighted that $(Na_2O + K_2O + CaO)/SiO_2$ has a significant influence on the electrical conductivity of granite samples at high temperatures and pressure. The impurity conduction is possible charge carriers such as K^+, Na^+, Ca^{2+} H^+),

which have lower conduction mechanisms. In comparison, Ionic conduction is possible charge carriers such as K^+ Na^+ and Ca^{2+} and higher conduction mechanisms at higher temperature ranges.

Due to the interest of environmental health and safety, the urban heat island impact, solar radiation, and air temperature during summer were measured, and the results are presented in Figs.10 for all samples, respectively. There is a clear indication that at 00:00 hrs, the urban heat island effect is the lowest because temperatures are low, leading to low radiation and low pavement temperatures. The curve shows that the pavement temperature rises from 07:00 hrs peeking at midday. It gradually drops until it gets cool after 19:00 hrs. It can be seen that pavement surface temperatures has a similar pattern with the curves for solar radiation and consequently the curve trend for air temperature. When the pavement surface temperature increases, the heat energy will be emitted to the environment. The speed of thermal cracking is influenced by the daily pavement amplitude of temperature variation (i.e. highest and lowest daily temperature at the pavement top layer) and temperature slope along the pavements depths. Pavement surface temperature relates to the urban heat island impact during summer and significantly impacts the rutting distress. The asphalt binder becomes less viscous at high temperatures and affects the adhesion between aggregates and bitumen. Note that the focus was on summer temperatures because Botswana is a semi-arid area temperature with relatively cool temperatures (0°C) during winter.

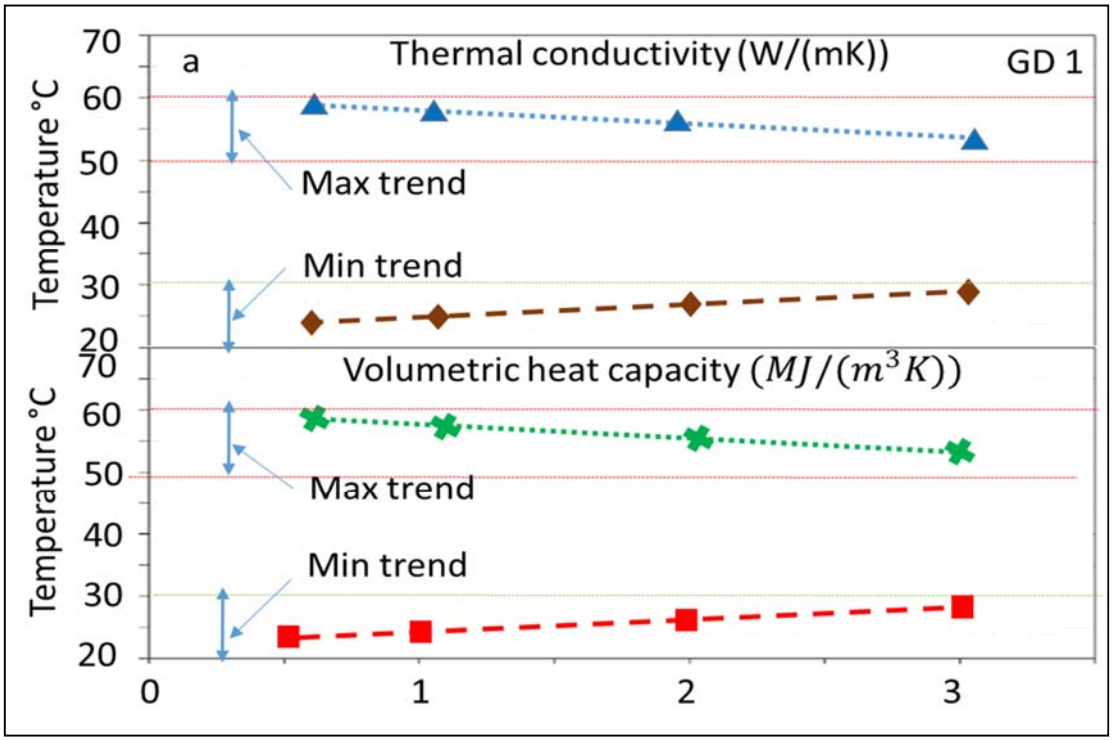
a
Thermal conductivity (W/(mK))
GD 1
Temperature °C
70
60
50
40
30
20
Max trend
Min trend
Volumetric heat capacity $(MJ/(m^3K))$
Max trend
Min trend
0
1
2
3

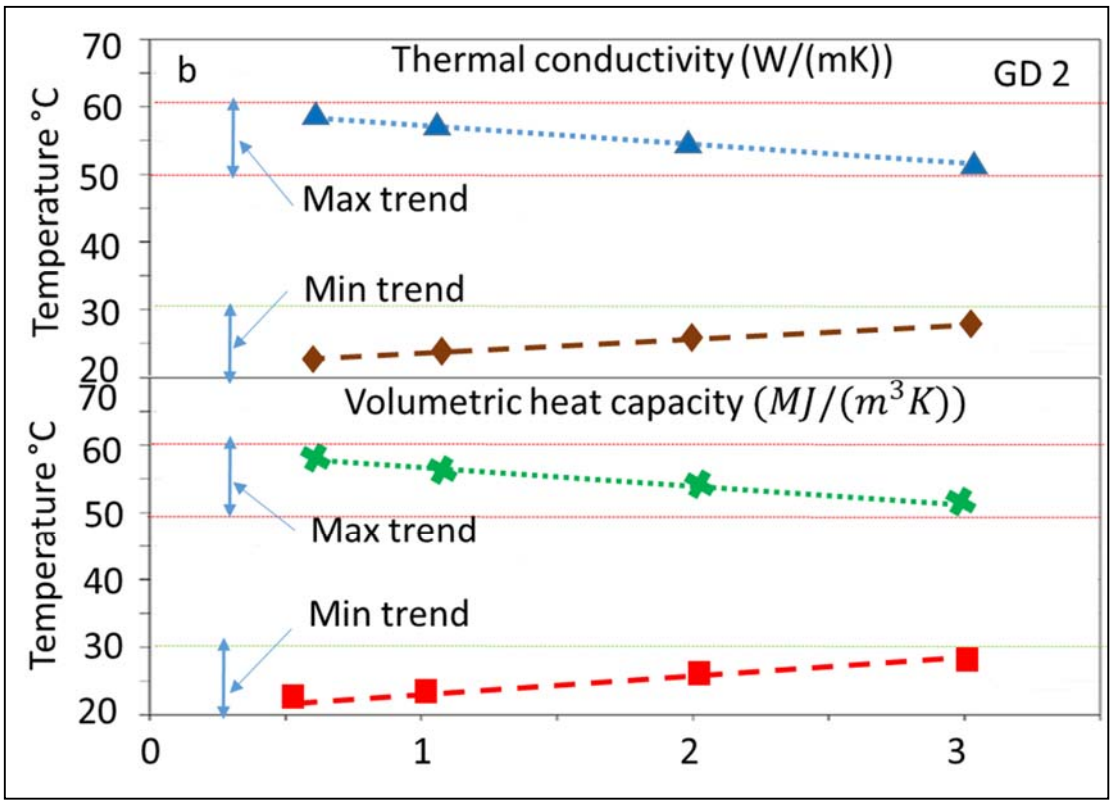
b
Thermal conductivity (W/(mK))
GD 2
Temperature °C
70
60
50
40
30
20
Max trend
Min trend
Volumetric heat capacity $(MJ/(m^3K))$
Max trend
Min trend
0
1
2
3

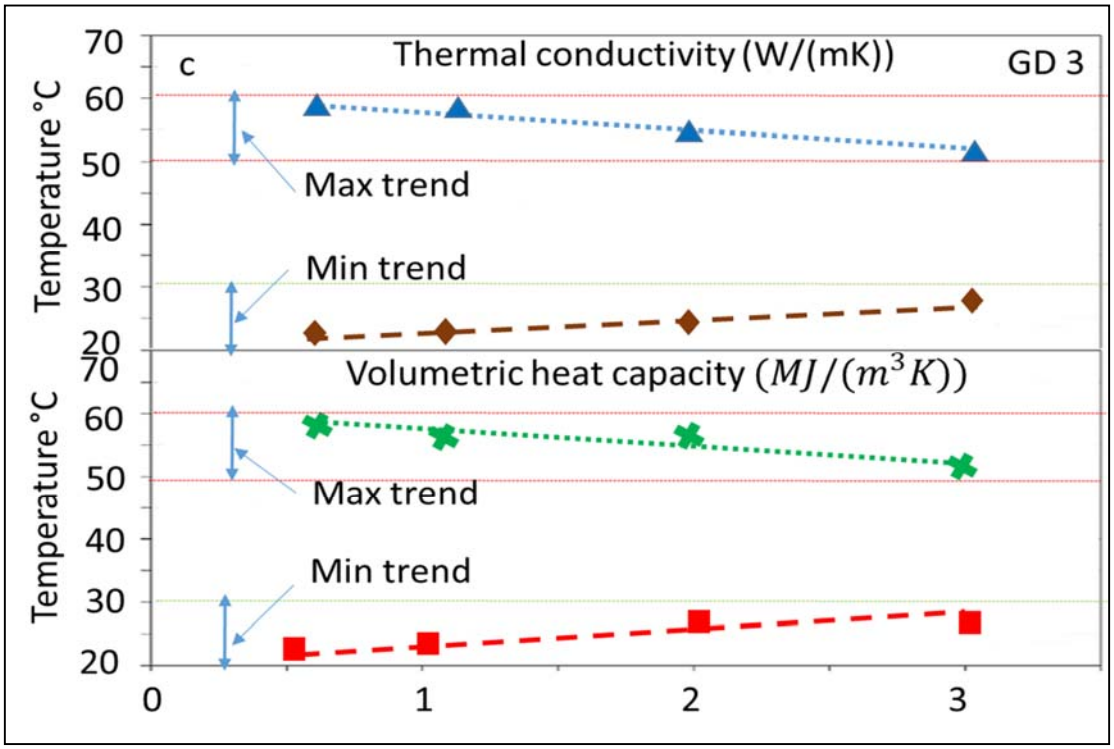

Figure 9: The highest and lowest the daily surface temperature: (a) difference of the thermal conductivity in summer, (b) difference of the volumetric heat capacity in summer

The dynamic stability order for these selected samples is GD 1, GD 2, and GD 3, and the deformation percentage order is GD 1, GD 2 and GD 3, respectively.

Table 7 presented the contact number correlation with Marshall stability and showed the maximum value for the stability of 8.4 kN, 7.4 kN, and 7.1 kN for GD 1, GD 2 and GD 3, respectively. GD 1, GD 2 and GD 3 strengths are relatively the same, and they provide high stability because of the angular shapes or high contact point number. GD 1 and GD 2, granite mixture, have better stability than GD 3. A high number of contact line lengths and texture of granite provide a good interlooking structure with the ability to transfer load easily among aggregates. Several studies have made a similar observation that angular aggregate particles improve the structural stability of asphalt mixture [56], [57]. As shown in Table 7, GD 1, GD 2, and GD 3 samples have higher Marshall ratios of 3.18, 2.72 and 2.63, respectively, representing the ratio of Marshall stability to flow value. Few studies have highlighted that

high Marshall stability indicates high stiffness, thus resistance to permanent deformation [42], [58]. As indicated in Table 7, results obtained from the three-point bending test were -197, 165 and 151 at temperature10 °C and 1745, 1700 and 1650 at temperature 0 °C for GD 1. GD 2 and GD 3. These results indicate that The GD 1 samples have the highest bending stiffness modulus at 10 °C, followed by GD 2 and GD 3, respectively, for 10°C and 0°C. Also, all mixtures have a recommendable influence at 10 °C and 0 °C, respectively. Granite, like Portland cement, contains SiO_2, $Al2O_3$, K_2O and CaO prove to have higher external compression force resistance.

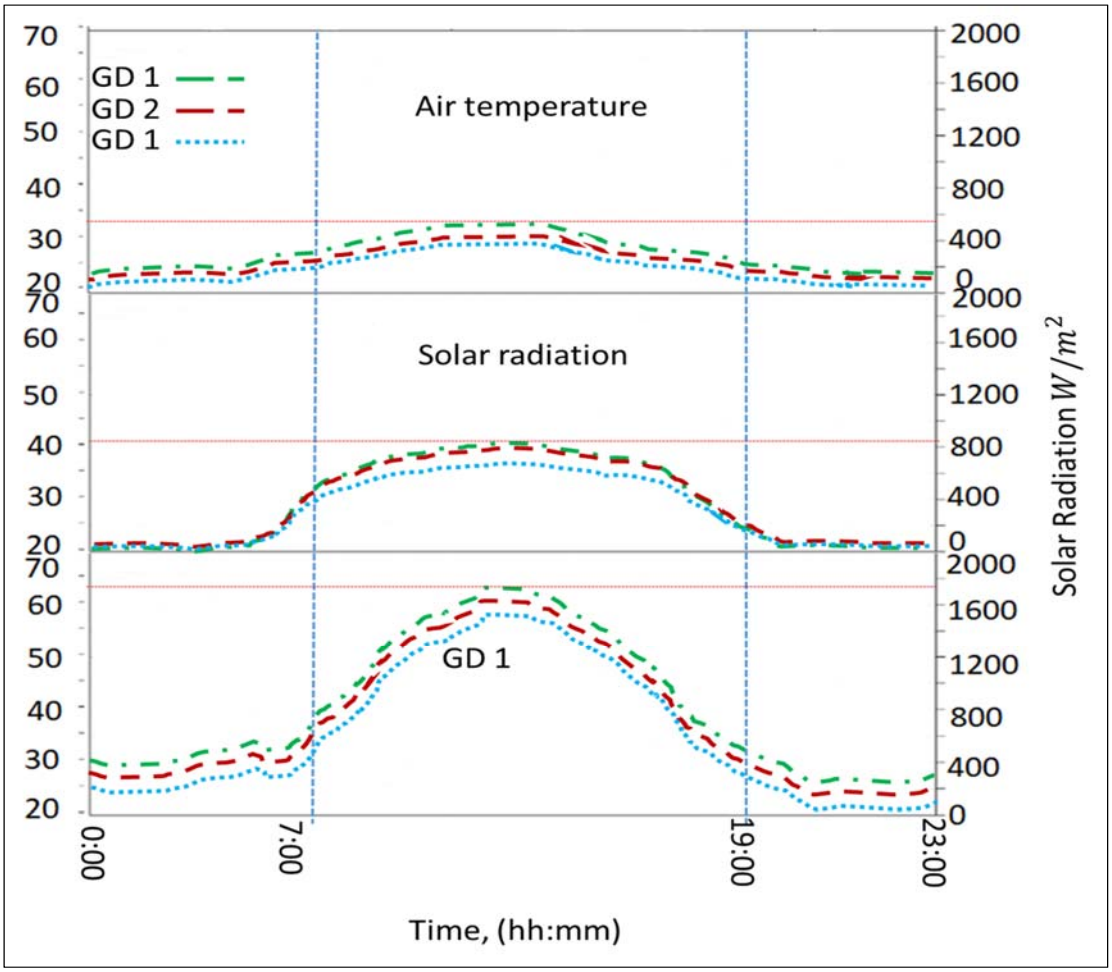

Fig. 10: The urban heat island impact, solar radiation, and air temperature for all mixtures

Table 7: Number of contact points and mechanical properties

	GD 1	GD 2	GD 3
	N_c		
	253	246	248
	Mechanical Properties		
Marshall Stability (kN)	8.4	7.6	7.1
Martial Ratio (kN/mm)	3.18	2.72	2.63
Rut Depth (mm)	1.32	1.36	1.51
Dynamic Stability (passes/mm)	9750	8218	6923
SB (MPa) 10 °C	197	165	151
SB (MPa) 0 °C	1745	1700	1650

Granite has excellent Marshall stability and a low flow of cubical shaped particles that easily contact each other and form a good microstructure. Generally, limestone has a spherical shape that provides less internal friction between aggregates and contains fewer pozzolanic elements such as Al_2O_3 and SiO_2, improving aggregate-binder adhesion while lowering bitumen stiffness (softening).

The anisotropy of the solid phase of the aggregate structure was quantified using F (a graphical and statistical approach) in a vector form. It can be observed from Figs. 11a, 11b and 11c present the linear F relation with Marshall stability, dynamic stability and stiffness modulus. R^2 for dynamic stability is 0.9048, 0.9032 and 0.921 for GD 1, GD 2 and GD 3, respectively. The R^2 bending stiffness modulus at temperature 10 °C is 0.918, 0.932 and 0.9132 for GD 1, GD 2 and GD 3, respectively. At temperature 0°C is 0.949, 0.934 and 0.930 for GD 1, GD 2 and GD 3, respectively. Granite aggregates exhibit a cubical shape with a large number of contacts point and a high contact line to provide a good interlocked aggregate structure that, under repeated stress, will not easily slip and change the tangential plane. Limestone with more of spherical shape has less texture to give stability like granite. Sukhwani et al. [59] used image analysis technologies to determine angularity and texture gradient for granite and limestone. They found that granite aggregates have a high texture and, thus, demonstrated better adherence

characteristics with asphalt binder than limestone aggregates with lower angularity and lower texture gradients. These results suggest a recommendable linear relationship between F with dynamic stability and bending stiffness modulus. There is evidence that F provides an alternative way to analyse the microstructure to examine the mechanical properties of asphalt mixture to a reasonable and comprehensive extent. For the asphalt mixtures to carry a high load, aggregate particles must be supported, at least the contact angle at approximately 90°. The aggregate skeleton has a major influence on the mechanical properties and durability of the asphalt mixture [60], [61]. Table 6, wheel tracking test results show the DS value, 9750, 8218, and 6923 passes/mm for GD 1, GD 2 and GD 3 samples. These results indicate the highest value for GD 1 samples and the lowest for GD 3 samples. The recorded values for rutting depth were 1.32 mm, 1.36 mm and 1.51 mm. This indicates that the GD 1 samples have the lowest rutting depth, and the GD 3 has the highest rut depth value in return. The values are above the standard specification of 2800 passes/mm [29]. This suggests a good performance by all mixtures at high-temperature areas [3]. For past studies with a similar aim, the results have shown a similar trend shown in this study [3], [62].

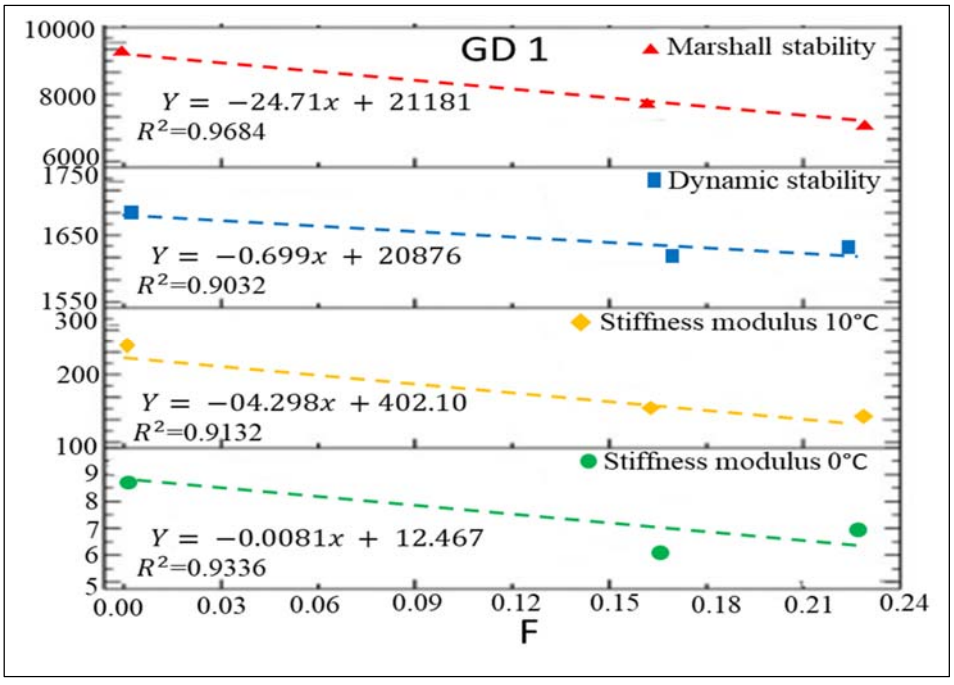

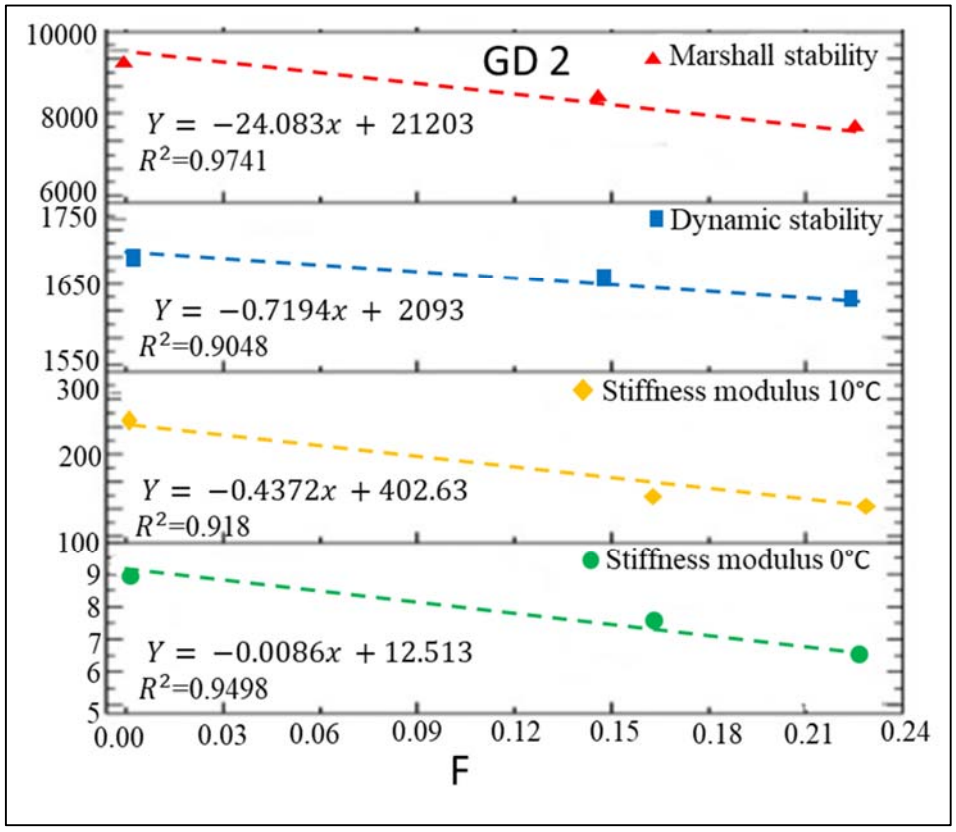

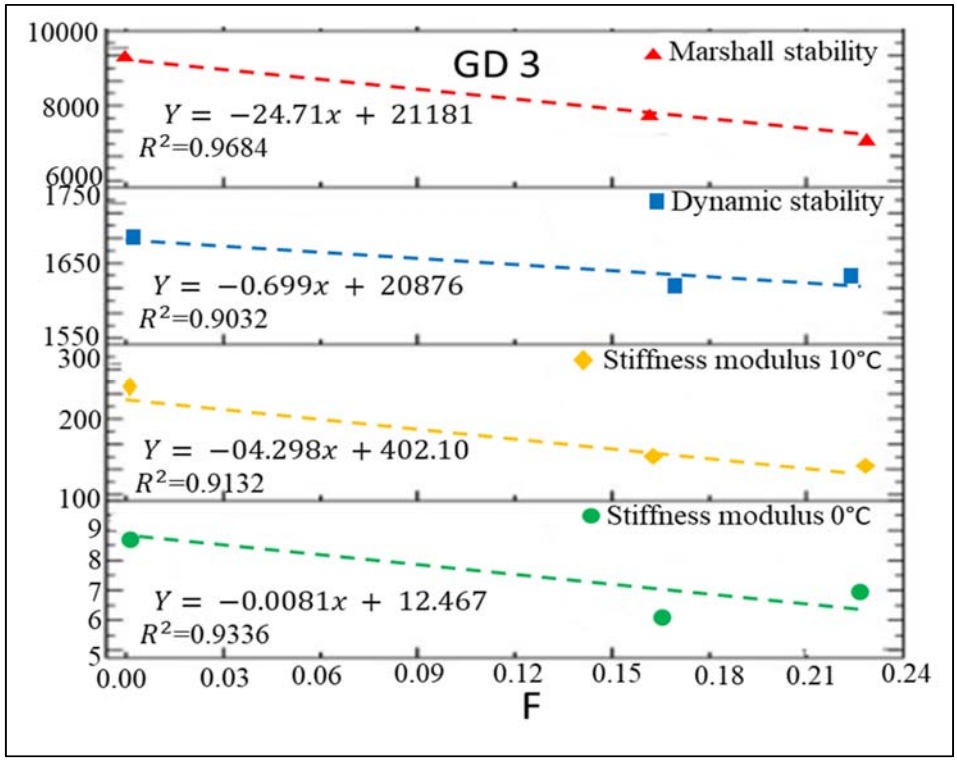

Figs.11, 11b and 11c: Correlation between F and Marshal stability, dynamic stability and stiffness modulus

This study generated the complex Poisson's ratio's master curves using the complex modulus test. Fig. 12 depicts the change in frequency and temperature significantly influencing the complex Poisson's ratio norm. Several studies found similar observations; results from the norm of the complex Poisson's ratio showed a clear, dynamic dependency on the frequency and temperature [63], [64]. At low temperature and high frequency, the value of |v*| raised by about 0.15, 0.13, and 0125 for GD 1, GD 2, and GD 3, respectively. At high temperature and low-frequency values of ϕ_v are raised with 0.45, 0.4 and 0.35 for GD 1, GD 2, and GD 3, respectively. It can be seen that the phase angles have very small and, to an extent, negative (except for only a few angles at high temperature). It can be seen that GD 1 samples had a better complex Poisson's ratio, followed by GD 2 and GD 3 been the lowest among the three types of samples, which suggest that the higher the aggregate contact, the higher the stiffness modulus. Both GD 1 and GD 2 are granite aggregate samples, but GD 1 has higher strength, contact point number, and better F than GD 2. This indicates that aggregate strength and shape can influence the nature of different rock sources and the environment.

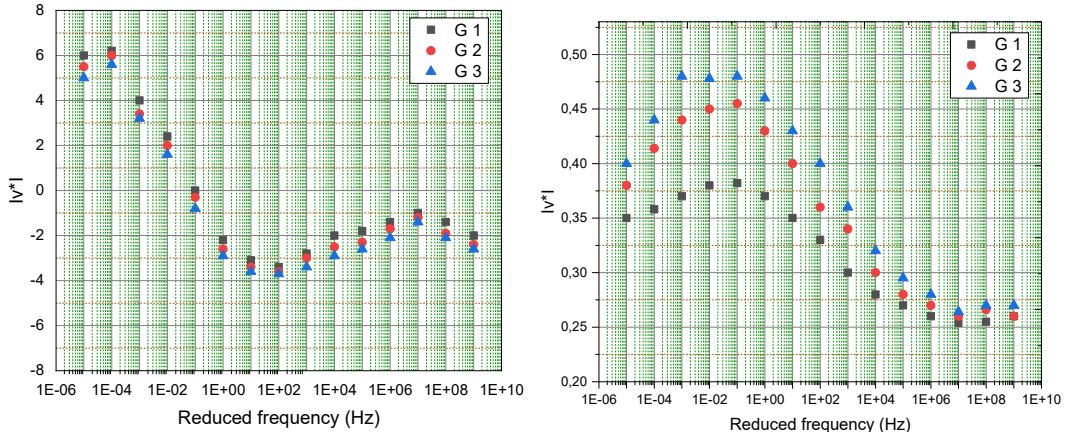

Fig. 12: Master curves of the complex Poisson's ratio of GD 1, GD 2 and GD 3 asphalt (a)mixtures for norm and (b) phase angle

Poisson's ratio parameter is always assumed to be constant in pavement engineering; this assumption always causes some errors because the parameter plays a good role performance

of civil engineering structure. Pouget et al. [65] performed a simulation to analyse the effect of time-frequency reliant on linear viscoelastic Poisson ratio. The results indicated that the behaviour of the orthotropic steel bridge has some variation. Figs. 11a and 11b, with the master curves such as a norm and phase angle, depict evidence of the time-temperature superposition principle (TTSP) on the complex Poisson's ratio. In this study, the identical alteration factors a_T was utilised used to generate the complex modulus and the complex Poisson's ratio's master curves. Several researchers to the same conclusion [39], [40], [64]. Granite has the highest pozzolanic elements such as Al_2O_3 and SiO_2 to enhance the adhesion strength between aggregate and bitumen bonds. On the other hand to granite has a lower CaO chemical composition than limestone, reducing bitumen stiffness. Thus, an indication that when low CaO content and high Al_2O_3 and SiO_2 are combined, it leads to increased bitumen softening, henceforth improving aggregate coating during the mixing procedure.

The study applied the stress of 100 kPa, 200 kPa, 300 kPa, and 400 kPa to evaluate the fatigue accumulated strain against creep permanent strain and stiffness modulus, as shown in Figs. 13a, 13b and 13c for GD 1, GD 2 and GD 3, respectively. It very well may be seen that the weakness amassed strain of the samples leads to a close connection with the creep permanent of the mixes. These results are consistent with the results from dynamic stability because GD 1 always show the highest stiffness modulus, followed by GD 2 and GD 3 as the least. GD 1 has high contact point weight, thus higher weight contact followed by GD 2 and GD 3.

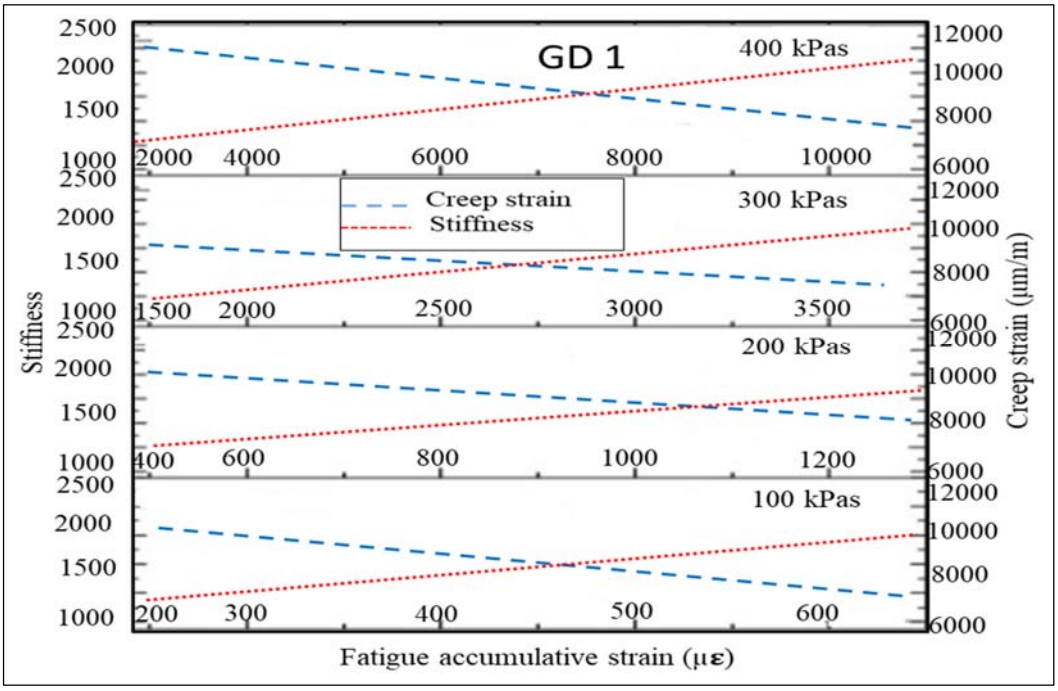
GD 1
400 kPas
300 kPas
200 kPas
100 kPas
Creep strain
Stiffness
Stiffness
Creep strain (μm/m)
Fatigue accumulative strain (με)

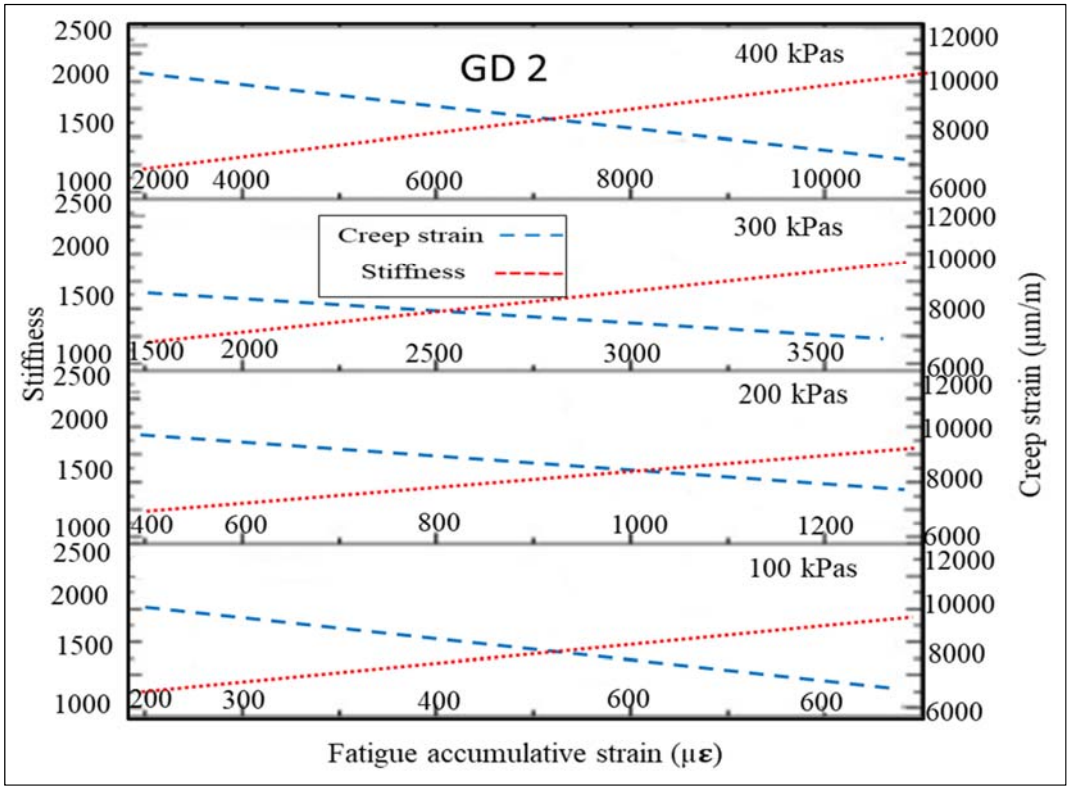
GD 2
400 kPas
300 kPas
200 kPas
100 kPas
Creep strain
Stiffness
Stiffness
Creep strain (μm/m)
Fatigue accumulative strain (με)

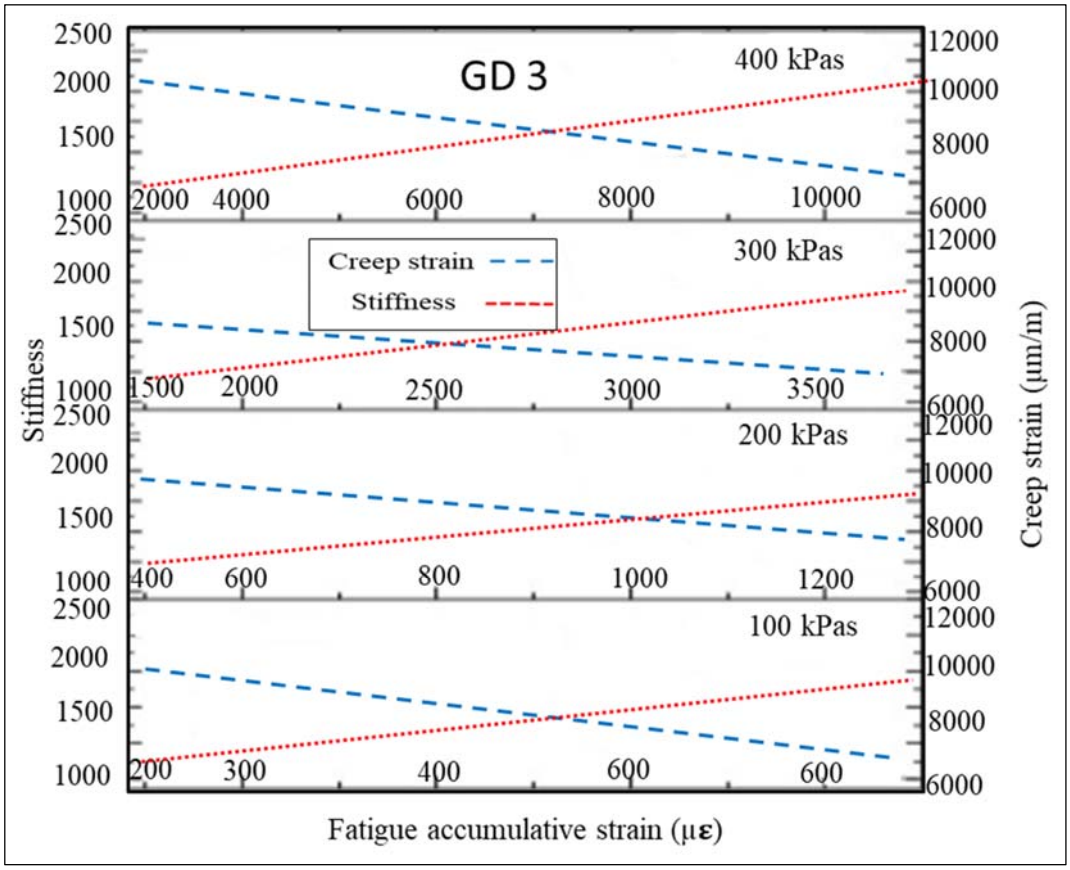

Fig 13: Correlation between fatigue accumulative strain with stiffness modulus and creep strain for (a) GD 1, (b) GD 2 and (c) GD 3

The results showed that the fatigue accumulated strain of the samples resulted in a correlation with the creep strain of the mixes. In contrast, an inverse correlation was obtained between the fatigue and stiffness properties. The results have shown that the less fatigue accumulated strain due by granite provided a decreased creep strain of the GD 1 and increased the stiffness properties.GD 3 asphalt mixture has higher accumulative fatigue and low creep modulus than GD 1 and GD 2 asphalt mixture. Granite with lower accumulative micro-strain leads to higher creep modulus, indicating low rutting potential. The results indicate a correlation of higher stability and lower flow of GD 1 and GD 2 compared to GD 3, as granite is mainly composed of SiO_2, $Al2O_3$, K_2O, and a small amount of CaO, which is a similar composition to Portland cement.

In order to statistically analyse the influence of physical and chemical properties of aggregates on the microstructural properties and mechanical performance, the Grey relational grade analysed to closer to one (1); or else, the grey relational grade will be analysed closer to zero (0). Chemical compositions such as SiO_2, $Al2O_3$, K_2O, and CaO, strength property of aggregates including CV and LAA, daily temperature variation and mechanical properties such as Marshall stability, dynamic stability, bending point beam at different temperatures and complex Poisson ratio were incorporated for the grey relational analysis. Table 8, Table 9 and Table 10 present data normalisation and Grey relational coefficients, respectively and grey relational grade, respectively. Results indicate that GD 1 and GD 2 have the highest values of Grey relational coefficients, equivalent to 1, and the least was GD 3 in all of the microstructure and mechanical performance indices, therefore suggesting that granites are granites have a good mechanical performance. The results showed that SiO_2, $Al2O_3$, K_2O, and a small amount of CaO significantly influence the shape and strength. The aggregates structure will affect the surface roughness, which will affect adhesion to bitumen. GD 1 is ranked 1, indicating excellent performance led by its roughest texture and cubical shape with many contacts points and longer contact line length. Consequently, high contact normal fabric tensors led to high stability. GD 2 as granite is ranked 2 because of its similar chemical and physical properties but a little bit less GD 1. GD 3 showed the least ranking.

Table 8: Data normalization

Material	Chemical composition				Strength		Microstructural properties		Environmental condition	Mechanical properties				
	Na2O	K2O	CaO	SiO2	C.V	LAA	N_c	F	DT	MS	DS	BP 0°C	BP 0°C	CPR
GD 1	0.335	0.335	0.212	0.315	0.079	0.098	1.000	1.000	1.000	1.000	1.000	1.000	1.000	1.000
GD 2	0.014	0.021	0.318	0.300	0.065	0.034	0.900	1.000	1.000	1.000	1.000	1.000	1.000	1.000
GD 3	0.190	0.080	0.200	0.280	0.035	0.200	0.430	0.100	0.027	0.080	0.100	0.010	0.042	0.150

Note DT = Daily temperature variation, MS = Marshall stability, DS = Dynamic stability, BP = Bending point, CPR = Complex Poisson ratio

Table 9: Grey relational coefficient

Material	Chemical composition				Strength		Microstructural properties		Environmental condition	Mechanical properties				
	Na2O	K2O	CaO	SiO2	C.V	LAA	N_c	F	DT	MS	DS	BP 0°C	BP 0°C	CPR
GD 1	0.126	0.144	0.014	0.098	0.388	0.365	1.000	1.000	1.000	1.000	1.000	1.000	1.000	1.000
GD 2	0.098	0.122	0.111	0.212	0.245	0.314	1.000	1.000	1.000	1.000	1.000	1.000	1.000	1.000
GD 3	0.100	0.010	0.000	0.167	0.000	0.234	0.356	0.467	0.366	0.370	0.350	0.334	0.343	0.340

Table 10:Grey relational degree

Grey relational analysis	GD 1	GD 2	GD 3
Chemical composition – strength	0.721	0.691	0.512
Chemical composition - microstructural properties	0.700	0.646	0.536
Chemical composition - mechanical properties	0.647	0.613	0.582
Strength - microstructural properties	0.564	0.501	0.453
Microstructural properties - mechanical properties	0.556	0.510	0.467
Chemical composition and strength -microstructural properties	0.819	0.723	0.634
Chemical composition and strength -mechanical properties	0.855	0.656	0.600
Ranking	1	2	3

5 Conclusion

This study prepared asphalt mixture using aggregates from three different sources (GD 1, GD 2, and GD 3), which were collected from three quarries in different parts of Botswana. The chemical oxide composition of the GD 1 and GD 2 as granite samples has shown that silicon, calcium, and aluminium are the three major elements in the granite aggregate particles. The major chemical oxide composition of GD 3 is SiO_2, $Al2O_3$, K_2O and CaO. Microstructural properties were captured using a charge-coupled device (CCD) digital camera and analysed by iPAS software. The properties aggregates shape properties such as the contact points N_c, the contact line and the contact orientation /discrete directional contact normal. These properties were used to calculate indices such as $E(n)$ and N and lastly F. The influence of contact number, length and F on inherent and stress-induced anisotropic properties of asphalt mixture were evaluated using the Marshall test, a wheel track test and three bending tests to assess Marshall stability, rut depth, dynamic stability. In addition, samples were put under the sinusoidal loading to determine the complex modulus and complex Poisson's ratio of asphalt mixtures. The conclusions are outlined as follows:

- GD 1 has the highest amount of silicon and aluminium, hence the good compaction and highest strength, followed by GD 2, and the least was GD 3.
- A well compacted and high-strength aggregate rock increased the contact points weight for the aggregate particles whereas surface texture increased friction and enhanced the interlocking of the aggregate particles. A reasonable amount of silicon and aluminium in the filler provided a high amount of pozzolan, thus enhancing the mastic strength.

The number of aggregates orientation increases with the amount of contact weight of microstructure of asphalt mixtures, creating an enhanced stress distribution, hence less stress concentration

- The contact weight of aggregate particles influences the microstructural properties of the asphalt mixture. Deformation of the asphalt mixture due to loading becomes less when the loading direction is near the aggregate contact plane orientation.

- High contact weight notably impacts the Marshall stability, rutting depth, dynamic stability, and stiffness modulus at high and low temperatures. All samples showed good mechanical performance at all temperatures because of the high contact weight of the aggregate particles.

CRediT authorship contribution statement

Selinah Busang: Experiment work and numerical analysis and draft manuscript**.** James Maina: Discussion of the experimental work and numerical analysis and revision of the manuscript.

Declaration of Competing Interest

The authors declare that they have no known competing financial interests or personal relationships that could have appeared to influence the work reported in this paper.

Acknowledgement

The authors would like to acknowledge the partial support provided by the Managing Director of Bango Trading Moffat James in Botswana. The authors acknowledge the financial support from the Matswele plant hire.

References

[1] J. Chen, B. Huang, and X. Shu, "Air-Void Distribution Analysis of Asphalt Mixture Using Discrete Element Method," *J. Mater. Civ. Eng.*, vol. 25, no. 10, pp. 1375–1385, 2013.

[2] M. Mohammed, T. Parry, N. Thom, and J. Grenfell, "Microstructure and mechanical properties of fibre reinforced asphalt mixtures," *Constr. Build. Mater.*, vol. 240, p. 117932, 2020.

[3] H. M. Z. Hassan *et al.*, "Study on the influence of aggregate strength and shape on the performance of asphalt mixture," *Constr. Build. Mater.*, vol. 294, p. 123599, 2021.

[4] B. Rajan and D. Singh, “Comparison of Shape Parameters and Laboratory Performance of Coarse Aggregates Produced from Different Types of Crushing Operations,” *J. Mater. Civ. Eng.*, vol. 29, no. 7, p. 04017044, 2017.

[5] D. Han, M. Yuan, and H. Hu, “Establishing prediction master curve of dynamic modulus of asphalt mixture considering randomness of aggregate morphology,” *Constr. Build. Mater.*, vol. 294, p. 123575, 2021.

[6] S. L. L. X.H. Yang, Y.Q. Bi, J.P. Zhang, “Impacts of aggregate morphological characteristics on asphalt mixture performance based on experimental tests,” *4th Geo-China Int. Conf. Sustain. Civ. Infrastructures - Innov. Technol. Sev. Weather. Clim. Chang. Shandong*, vol. 266, pp. 34–41, 2016.

[7] D. Kuang, X. Wang, Y. Jiao, B. Zhang, Y. Liu, and H. Chen, “Influence of angularity and roughness of coarse aggregates on asphalt mixture performance,” *Constr. Build. Mater.*, vol. 200, pp. 681–686, 2019.

[8] J. Gao *et al.*, “Influence of Coarse-Aggregate Angularity on Asphalt Mixture Macroperformance : Skid Resistance , High-Temperature , and Compaction Performance,” *Am. Soc. Civ. Eng.*, vol. 32, no. 2011, pp. 1–11, 2020.

[9] H. Ge, A. Sha, Z. Han, and X. Xiong, “Three-dimensional characterization of morphology and abrasion decay laws for coarse aggregates,” *Constr. Build. Mater.*, vol. 188, pp. 58–67, 2018.

[10] H. Wang, Y. Bu, Y. Wang, X. Yang, and Z. You, “The effect of morphological characteristic of coarse aggregates measured with fractal dimension on asphalt mixture’s high-temperature performance,” *Adv. Mater. Sci. Eng.*, vol. 2016, 2016.

[11] M. Shaheen, A. Al-Mayah, and S. Tighe, “A novel method for evaluating hot mix asphalt fatigue damage: X-ray computed tomography,” *Constr. Build. Mater.*, vol. 113, pp. 121–133, 2016.

[12] H. Behbahani, “Evaluation of Fatigue and Rutting Behaviour of Hot Mix Asphalt Containing Rock Wool,” *Int. J. Civ. Eng.*, vol. 18, no. 11, pp. 1293–1300, 2020.

[13] L.-L. F. Yu, “Petrography,” *(Moscow Publ. House Acad. Sci. USSR)*, p. 447., 1955.

[14] T. Yi-qiu, X. Li, and X. Zhou, “Interactions of Granite and Asphalt Based on the Rheological Characteristics,” *J. Mater. Civ. Eng.*, vol. 22, no. 8, pp. 820–825, 2010.

[15] H. Hu, “The influence of granite microstructure on the properties of pavement material,” *2011 Int. Conf. Electr. Technol. Civ. Eng.*, pp. 6311–6314, 2011.

[16] S. Yefremov, “Influence of genesis of mineral components of asphalt concrete for its durability in aggressive environments,” *IOP Conf. Ser. Mater. Sci. Eng.*, vol. 907, no. 1, 2020.

[17] J. Fonseca, C. O’Sullivan, M. R. Coop, and P. D. Lee, “Quantifying the evolution of soil fabric during shearing using directional parameters,” *Geotechnique*, vol. 63, no. 6, pp. 487–499, 2013.

[18] D. Mašín, C. Tamagnini, G. Viggiani, and D. Costanzo, “Fabric evolution within shear bands of granular materials and its relation to critical state theory,” *Int. J. Numer. Anal. Methods Geomech.*, vol. 30, no. 13, pp. 1303–1336, 2006.

[19] R. Yuan, H. S. Yu, D. S. Yang, and N. Hu, "On a fabric evolution law incorporating the effects of b-value," *Comput. Geotech.*, vol. 105, no. October 2017, pp. 142–154, 2019.

[20] J. Shi and P. Guo, "Induced fabric anisotropy of granular materials in biaxial tests along imposed strain paths," *Soils Found.*, vol. 58, no. 2, pp. 249–263, 2018.

[21] B. S. Underwood, Y. R. Kim, B. S. Underwood, and Y. R. Kim, "Microstructural investigation of asphalt concrete for performing multiscale experimental studies," *Int. J. Pavement Eng.*, vol. 8436, pp. 1029–8436, 2013.

[22] A. Adu-Osei, "Characterization of unbound granular layers in flexible pavements. Report No.ICAR/502-3," 2000.

[23] E. Masad, L. Tashman, D. Little, and H. Zbib, "Viscoplastic modeling of asphalt mixes with the effects of anisotropy, damage and aggregate characteristics," *Mech. Mater.*, vol. 37, no. 12, pp. 1242–1256, 2005.

[24] S. H. Kim, D. N. Little, and E. Masad, "Simple methods to estimate inherent and stress-induced anisotropy of aggregate base," *Transp. Res. Rec.*, no. 1913, pp. 24–31, 2005.

[25] N. P. Kruyt, I. Agnolin, S. Luding, and L. Rothenburg, "Micromechanical study of elastic moduli of loose granular materials," *J. Mech. Phys. Solids*, vol. 58, no. 9, pp. 1286–1301, 2010.

[26] Y. H. Xie, Z. X. Yang, D. Barreto, and M. D. Jiang, "The influence of particle geometry and the intermediate stress ratio on the shear behavior of granular materials," *Granul. Matter*, vol. 19, no. 2, pp. 1–13, 2017.

[27] D. Mašín, C. Tamagnini, G. Viggiani, and D. Costanzo, "A critical state sand plasticity model accounting for fabric evolution," *Int. J. Numer. Anal. Methods Geomech.*, vol. 30, no. 13, pp. 1303–1336, 2006.

[28] X. Li, H. S. Yu, and X. S. Li, "International Journal of Solids and Structures Macro – micro relations in granular mechanics," *Int. J. Solids Struct.*, vol. 46, pp. 4331–4341, 2009.

[29] "Ministry of Transport, Standard Test Methods of Bitumen and Bituminous Mixtures for Highway Engineering, in: China Commun. Press, China Communications Press, Beijing, China, 2011: pp. 1–370," 2011.

[30] Government of Botswana, "Botswana Environment Statistics Climate Digest," *Report*, no. March, pp. 1–21, 2019.

[31] X. Shi, Y. Rew, E. Ivers, C. S. Shon, E. M. Stenger, and P. Park, "Effects of thermally modified asphalt concrete on pavement temperature," *Int. J. Pavement Eng.*, vol. 8436, pp. 1–13, 2017.

[32] *ASTM D6927, American Society for Testing and Materials, Standard test method for Marshall stability and flow of asphalt mixtures, 2015, Washington, DC.* 2015.

[33] R. Guo and T. Nian, "Analysis of factors that influence anti-rutting performance of asphalt pavement," *Constr. Build. Mater.*, vol. 254, p. 119237, 2020.

[34] X. Cai, D. Wang, W. Huang, J. Yu, and C. Wan, "Evaluation of Rutting Performance

of Asphalt Mixture with Driving Wheel Pavement Analyzer," *Adv. Mater. Sci. Eng.*, vol. 2017, 2017.

[35] C. Kuo and R. B. Freeman, "Imaging Indices for Quantification of Shape , Angularity , and Surface Texture of Aggregates," *Transp. Res. Rec. 1721*, no. 00–0686, pp. 57–65.

[36] "ASTM D6926, American Society for Testing and Materials, Standard practice for preparation of bituminous specimens using Marshall apparatus, 2010, Washington, DC.," p. 6926, 2010.

[37] M. Miljkovic and M. Radenberg, "Rutting mechanisms and advanced laboratory testing of asphalt mixtures resistance against permanent deformation," *Facta Univ. - Ser. Archit. Civ. Eng.*, vol. 9, no. 3, pp. 407–417, 2011.

[38] Q. Tuan, H. Di, Q. Phuc, T. Thanh, and N. Hoang, "Effect of time – temperature , strain level and cyclic loading on the complex Poisson ' s ratio of asphalt mixtures," *Constr. Build. Mater.*, vol. 294, p. 123564, 2021.

[39] Q. T. N. . H. D. B. . S. Cedri, "Linear and nonlinear viscoelastic behaviour of bituminous mixtures," *Mater. Struct.*, pp. 2339–2351, 2015.

[40] D. B. Ce *et al.*, "3Dim experimental investigation of linear viscoelastic properties of bituminous mixtures," pp. 4813–4829, 2016.

[41] H. Xiao *et al.*, "Analysis of Composite Skeleton Characteristics of Recycled Asphalt Mixture via Weight Analysis Method," *Front. Mater.*, vol. 7, Jul. 2020.

[42] X. Cai, K. H. Wu, W. K. Huang, and C. Wan, "Study on the correlation between aggregate skeleton characteristics and rutting performance of asphalt mixture," *Constr. Build. Mater. J.*, vol. 179, pp. 294–301, 2018.

[43] J. Jiang, F. Ni, L. Gao, and L. Yao, "Effect of the contact structure characteristics on rutting performance in asphalt mixtures using 2D imaging analysis," *Constr. Build. Mater.*, vol. 136, pp. 426–435, 2017.

[44] N. R. Sefidmazgi, L. Tashman, and H. Bahia, "Internal structure characterization of asphalt mixtures for rutting performance using imaging analysis," *Road Mater. Pavement Des.*, vol. 13, no. SUPPL. 1, pp. 21–37, 2012.

[45] S. M., "Fabric tensor in granular materials.," in *Proceedings IUTAM conference on deformation and failure of granular materials, Delft;*, 1982, p. 1982.

[46] F. Tatsuoka, "Small strain behaviour of granular materials.: Introduct.," *Mech. Granul. Mater*, pp. 299 – 308, 1999.

[47] R. Wang, M. Asce, W. Cao, and J. Zhang, "Dependency of Dilatancy Ratio on Fabric Anisotropy in Granular Materials," *10.1061/(ASCE)EM.1943-7889.0001660*, vol. 145, no. 10, pp. 1–13, 2019.

[48] N. Hu, P. Z. Zhuang, D. S. Yang, and H. S. Yu, "On the evolution law of a contact normal-based fabric tensor for granular materials," *Comput. Geotech.*, vol. 132, no. February, p. 103857, 2021.

[49] A. N. Siddiquee and Z. A. Khan, "Grey relational analysis coupled with principal component analysis for optimisation design of the process parameters in in-feed centreless cylindrical grinding," *Int. J. Adv. Manuf. Technol.*, no. February, 2010.

[50] S. Yagüe, C. Gonz, V. R. Prieto, and S. Alberto, “Sustainable Ecocements : Chemical and Morphological Analysis of Granite Sawdust Waste as Pozzolan Material,” *MDPI, Mater.*, pp. 1–15, 2020.

[51] E. Arambula, “Influence of fundamental material properties and air void structure on moisture damage of asphalt mixes,” *Thesis, Dpoctor Philos. Civ. Eng. Texas A&M Univ.*, no. January, 2007.

[52] J. Gao *et al.*, “Effects of coarse aggregate angularity on the microstructure of asphalt mixture,” *Constr. Build. Mater.*, vol. 183, pp. 472–484, 2018.

[53] J. Chen, M. Zhang, H. Wang, and L. Li, “Evaluation of thermal conductivity of asphalt concrete with heterogeneous microstructure,” *Appl. Therm. Eng.*, vol. 84, pp. 368–374, 2015.

[54] A. E. Ramazanova and S. N. Emirov, “Baric and Temperature Dependences for the Thermal Conductivity of Sedimentary Rocks,” *Bull. Russ. Acad. Sci. Physics,* vol. 76, no. 10, pp. 1283–1287, 2012.

[55] L. Dai, H. Hu, H. Li, J. Jiang, and K. Hui, “Influence of temperature , pressure , and chemical composition on the electrical conductivity of granite,” *Am. Minerol. Geosci.*, vol. 99, no. 7, pp. 1420–1428., 2014.

[56] T. Pan, M. Asce, E. Tutumluer, M. Asce, S. H. Carpenter, and M. Asce, “Effect of Coarse Aggregate Morphology on Permanent Deformation Behavior of Hot Mix Asphalt,” *Am. Soc. Civ. Eng.*, vol. 132, no. 7, pp. 580–589, 2006.

[57] P. Li, J. Su, S. Ma, and H. Dong, “Effect of aggregate contact condition on skeleton stability in asphalt mixture,” *Int. J. Pavement Eng.*, vol. 8436, pp. 1–7, 2020.

[58] H. Xiao *et al.*, “Analysis of Composite Skeleton Characteristics of Recycled Asphalt Mixture via Weight Analysis Method,” *Struct. Mater. a Sect. J. Front. Mater.*, vol. 7, no. July, pp. 1–9, 2020.

[59] T. Report, D. Page, and P. Covered, “Sensitivity of hma performance to aggregate shape measured using conventional and image analysis methods,” *Report*, vol. 7, no. 2, 2006.

[60] E. Horak, H. Sebaaly, J. Maina, and S. Varma, “Relationship Between Bailey and Dominant Aggregate Size Range,” in *36th Southern African Transport Conference*, 2017, no. July, pp. 245–263.

[61] J. W. Maina, Y. Ozawa, and K. Matsui, “Axi-symmetric analyses of vertically inhomogeneous elastic multilayered systems,” *Bear. Capacit. Roads, Railw. Airfields - Proc. 8th Int. Conf. Bear. Capacit. Roads, Railw. Airfields*, vol. 1, pp. 561–570, 2009.

[62] N. S. Mashaan, M. R. Karim, M. A. Aziz, M. R. Ibrahim, H. Y. Katman, and S. Koting, “Evaluation of Fatigue Life of CRM-Reinforced SMA and Its Relationship to Dynamic Stiffness,” *Sci. World J.*, 2014.

[63] S. Pouget *et al.*, “From the Behavior of Constituent Materials to the Calculation and Design of Orthotropic Bridge Structures From the Behavior of Constituent Materials to the Calculation and Design of Orthotropic Bridge Structures,” *Road Mater. Pavement Des.*, vol. 0629, pp. 2164–0629, 2011.

[64] A. Graziani, M. Bocci, and F. Canestrari, “Complex Poisson ’ s ratio of bituminous

mixtures : measurement and modeling," *Mater. Struct.*, vol. 47, pp. 1131–1148, 2014.

[65] H. Di Benedetto and S. P. C. Sauze, "Modeling of viscous bituminous wearing course materials on orthotropic steel deck," *Mater. Struct.*, vol. 45, pp. 1115–1125, 2012.